with stage progression. Taken together, these data suggest that the level of EphA10 expression partly contributes to breast cancer progression.

Next, we evaluated the relationship between EphA10 protein expression and clinicopathological characteristics. Immunohistochemistry (IHC) staining of TMAs showed that EphA10 was expressed in approximately 60% of breast tumor tissues, but not in normal breast tissues, which is consistent with our previous studies [13] (Fig. 2).

Statistical analysis revealed that EphA10 expression at the protein level was also independent of age, gender, histological classification and pT indexes. However, EphA10 protein expression was positively associated LN metastasis and stage progression (Table 2). Moreover, in order to validate this correlation, we also performed an analysis using a different anti-EphA10 antibody that we had isolated from a naïve phage antibody library, which gave similar results (data not shown). In addition, we also analyzed the possible correlation between EphA10 protein level and LN metastasis or stage progression, using the IHC staining total score as an indicator of the protein expression level. As shown to Figure S1, the total score is significantly associated with LN metastasis, but not stage progression. Taken together, our findings indicate that EphA10 expression is related to LN metastasis as well as stage progression in breast cancer, although improved quantitative analysis of protein expression level by mass spectrometry is needed.

Other Eph receptors such as EphA2 or EphB3 have invasive, migrating and anoikis-inhibiting abilities, so that EphA2- or EphB3-expressing cancer cells promote metastasis [3, 9–11]. Thus, EphA10 could also elicit a similar biological effect on disease progression, although further investigations are needed to elucidate the mechanism by which EphA10 expression is correlated with LN metastasis. Moreover, aiming for LN metastasis prediction, we should set up the criteria by more sample analyses and evaluate LN metastasis prospectively.

In conclusion, we demonstrated that EphA10 expression at both the gene and protein level in clinical breast cancer tissues is significantly associated with LN metastasis as well as stage progression. We believe that the data will help elucidate the biological function of EphA10 and facilitate the development of novel breast cancer drugs.

Acknowledgments

This study was supported in part by Grants-in-Aid for Scientific Research and Project for Development of Innovative Research on Cancer Therapeutics from the Ministry of Education, Culture, Sports, Science and Technology of Japan. This study was also supported in part by Health Labor Sciences Research Grants from the Ministry of Health, Labor and Welfare of Japan.

Conflict of Interest

None declared.

References

1. Yamaguchi, Y., and E. B. Pasquale. 2004. Eph receptors in the adult brain. Curr. Opin. Neurobiol. 14:288–296.
2. Konstantinova, I., G. Nikolova, M. Ohara-Imaizumi, P. Meda, T. Kucera, K. Zarbalis, et al. 2007. EphA-Ephrin-A-mediated beta cell communication regulates insulin secretion from pancreatic islets. Cell 129:359–370.
3. Brantley-Sieders, D. M., G. Zhuang, D. Hicks, W. B. Fang, Y. Hwang, J. M. Cates, et al. 2008. The receptor tyrosine kinase EphA2 promotes mammary adenocarcinoma tumorigenesis and metastatic progression in mice by amplifying ErbB2 signaling. J. Clin. Invest. 118:64–78.
4. Munarini, N., R. Jager, S. Abderhalden, G. Zuercher, V. Rohrbach, S. Loercher, et al. 2002. Altered mammary epithelial development, pattern formation and involution in transgenic mice expressing the EphB4 receptor tyrosine kinase. J. Cell Sci. 115:25–37.
5. Mohammed, K. A., X. Wang, E. P. Goldberg, V. B. Antony, and N. Nasreen. 2011. Silencing receptor EphA2 induces apoptosis and attenuates tumor growth in malignant mesothelioma. Am. J. Cancer Res. 1:419–431.
6. Kumar, S. R., J. Singh, G. Xia, V. Krasnoperov, L. Hassanieh, E. J. Ley, et al. 2006. Receptor tyrosine kinase EphB4 is a survival factor in breast cancer. Am. J. Pathol. 169:279–293.
7. Sawamiphak, S., S. Seidel, C. L. Essmann, G. A. Wilkinson, M. E. Pitulescu, T. Acker, et al. 2010. Ephrin-B2 regulates VEGFR2 function in developmental and tumour angiogenesis. Nature 465:487–491.
8. Noren, N. K., M. Lu, A. L. Freeman, M. Koolpe, and E. B. Pasquale. 2004. Interplay between EphB4 on tumor cells and vascular ephrin-B2 regulates tumor growth. Proc. Natl Acad. Sci. USA 101:5583–5588.
9. Brantley-Sieders, D. M., W. B. Fang, D. J. Hicks, G. Zhuang, Y. Shyr, and J. Chen. 2005. Impaired tumor microenvironment in EphA2-deficient mice inhibits tumor angiogenesis and metastatic progression. FASEB J. 19:1884–1886.
10. Duxbury, M. S., H. Ito, M. J. Zinner, S. W. Ashley, and E. E. Whang. 2004. EphA2: a determinant of malignant cellular behavior and a potential therapeutic target in pancreatic adenocarcinoma. Oncogene 23:1448–1456.
11. Ji, X. D., G. Li, Y. X. Feng, J. S. Zhao, J. J. Li, Z. J. Sun, et al. 2011. EphB3 is overexpressed in

non-small-cell lung cancer and promotes tumor metastasis by enhancing cell survival and migration. Cancer Res. 71:1156–1166.
12. Annunziata, C. M., E. C. Kohn, P. Lorusso, N. D. Houston, R. L. Coleman, M. Buzoianu, et al. 2013. Phase 1, open-label study of MEDI-547 in patients with relapsed or refractory solid tumors. Invest. New Drugs 31:77–84.
13. Imai, S., K. Nagano, Y. Yoshida, T. Okamura, T. Yamashita, Y. Abe, et al. 2011. Development of an antibody proteomics system using a phage antibody library for efficient screening of biomarker proteins. Biomaterials 32:162–169.
14. Aasheim, H. C., S. Patzke, H. S. Hjorthaug, and E. F. Finne. 2005. Characterization of a novel Eph receptor tyrosine kinase, EphA10, expressed in testis. Biochim. Biophys. Acta 1723:1–7.

Supporting Information

Additional Supporting Information may be found in the online version of this article:

Figure S1. EphA10 protein expression level analysis in LN-positive and -negative cases, or stage I, II, and III.

Cytokine 61 (2013) 578–584

Contents lists available at SciVerse ScienceDirect

Cytokine

journal homepage: www.journals.elsevier.com/cytokine

Mutants of lymphotoxin-α with augmented cytotoxic activity *via* TNFR1 for use in cancer therapy

Tomohiro Morishige [a,1], Yasuo Yoshioka [b,c,*,1], Shogo Narimatsu [a], Shinji Ikemizu [d], Shin-ichi Tsunoda [c,e], Yasuo Tsutsumi [b,c,e], Yohei Mukai [a], Naoki Okada [a], Shinsaku Nakagawa [a,c,*]

[a] *Laboratory of Biotechnology and Therapeutics, Graduate School of Pharmaceutical Sciences, Osaka University, 1-6 Yamadaoka, Suita, Osaka 565-0871, Japan*
[b] *Laboratory of Toxicology and Safety Science, Graduate School of Pharmaceutical Sciences, Osaka University, 1-6 Yamadaoka, Suita, Osaka 565-0871, Japan*
[c] *The Center for Advanced Medical Engineering and Informatics, Osaka University, 1-6 Yamadaoka, Suita, Osaka 565-0871, Japan*
[d] *Graduate School of Pharmaceutical Sciences, Kumamoto University, 5-1 Oe-honmachi, Kumamoto 862-0973, Japan*
[e] *Laboratory of Biopharmaceutical Research, National Institute of Biomedical Innovation, 7-6-8 Saito-Asagi, Ibaraki, Osaka 567-0085, Japan*

ARTICLE INFO

Article history:
Received 6 July 2012
Received in revised form 29 September 2012
Accepted 6 November 2012
Available online 11 December 2012

Keywords:
Affinity
Apoptosis
Bioactivity
Cytokine
Cytotoxicity

ABSTRACT

The cytokine lymphotoxin-α (LTα) is a promising candidate for use in cancer therapy. However, the instability of LTα *in vivo* and the insufficient levels of tumor necrosis factor receptor 1 (TNFR1)-mediated bioactivity of LTα limit its therapeutic potential. Here, we created LTα mutants with increased TNFR1-mediated bioactivity by using a phage display technique. We constructed a phage library displaying lysine-deficient structural variants of LTα with randomized amino acid residues. After affinity panning, we screened three clones of lysine-deficient LTα mutant, and identified a LTα mutant with TNFR1-mediated bioactivity that was 32 times that of the wild-type LTα (wtLTα). When compared with wtLTα, the selected clone showed augmented affinity to TNFR1 due to slow dissociation rather than rapid association. In contrast, the mutant showed only 4 times the TNFR2-mediated activity of wtLTα. In addition, the LTα mutant strongly and rapidly activated caspases that induce TNFR1-mediated cell death, whereas the mutant and wtLTα activated nuclear factor-kappa B to a similar extent. Our data suggest that the kinetics of LTα binding to TNFR1 play an important role in signal transduction patterns, and a TNFR1-selective LTα mutant with augmented bioactivity would be a superior candidate for cancer therapy.

1. Introduction

Lymphotoxin-alpha (LTα) is a tumor necrosis factor (TNF) superfamily cytokine with tumor-cell-specific cytotoxic activity and immune-activating activity. LTα induces the expression of chemokines and adhesion molecules in endothelial cells, and plays a key role in lymph node neogenesis [1–3]. Schrama et al. [4,5] showed that systemic administration of LTα to a tumor-bearing mouse leads to the construction of ectopic lymphoid tissue within the tumor and the strong induction of tumor immunity in that lymphoid tissue, suggesting that the underlying mechanism of this cytokine's anti-tumor activity may be effective. Therefore, LTα has long been considered to be a promising candidate for an anti-cancer agent. However, the clinical use of LTα has been limited because of the protein's *in vivo* instability and proinflammatory side effects.

One of the most common ways to improve the therapeutic effects of proteins is to conjugate them with polyethylene glycol (PEG) in a process called PEGylation, or to conjugate them with other water-soluble polymers [6]. Because of the steric hindrance caused by the PEG molecule, PEGylation can prolong the plasma half-life of molecules and alter the tissue distribution of the conjugates compared with those of the native form. PEGylation of proteins is mostly nonspecific because it targets all of the lysine residues in the protein, some of which may be in or near an active site. As a result, PEGylation significantly reduces the specific

Abbreviations: E. coli, Escherichia coli; ELISA, enzyme-linked immunosorbent assay; FADD, Fas-associated protein with death domain; FBS, fetal bovine serum; HVEM, herpes virus entry mediator; IFNγ, interferon γ; LTα, lymphotoxin-alpha; NFκB, nuclear factor-kappa B; PEG, polyethylene glycol; pI, isoelectric points; SDS–PAGE, sodium dodecyl sulfate–polyacrylamidegel electrophoresis; SPR, surface plasmon resonance; TNF, tumor necrosis factor; TNFR1, TNF receptor 1; TRADD, TNF receptor-associated death domain; TRAF, TNF receptor-associated factor; wtLTα, wild-type LTα.

* Corresponding authors. Addresses: Laboratory of Toxicology and Safety Science, Graduate School of Pharmaceutical Sciences, Osaka University, 1-6 Yamadaoka, Suita, Osaka 565-0871, Japan. Tel./fax: +81 6 6879 8233 (Y. Yoshioka), Laboratory of Biotechnology and Therapeutics, Graduate School of Pharmaceutical Sciences, Osaka University, 1-6 Yamadaoka, Suita, Osaka 565-0871, Japan. Tel.: +81 6 6879 8175; fax: +81 6 6879 8179 (S. Nakagawa).

E-mail addresses: yasuo@phs.osaka-u.ac.jp (Y. Yoshiokab), nakagawa@phs.osaka-u.ac.jp (S. Nakagawa).

[1] These authors contributed equally to the work.

1043-4666/$ - see front matter © 2012 Elsevier Ltd. All rights reserved.
http://dx.doi.org/10.1016/j.cyto.2012.11.005

activity of the proteins involved. Our group previously developed a novel strategy for site-specific mono-PEGylation of lysine-deficient mutants to overcome these limitations of PEGylation [7,8]. We demonstrated that site-specific PEGylation of a lysine-deficient mutant of LTα retained higher bioactivity compared with random PEGylation of wild-type LTα (wtLTα) [9]. This finding suggests that site-specific PEGylation of a lysine-deficient mutant of LTα might be a useful way to overcome the problems in the clinical use of LTα outlined above.

LTα binds to three receptor subtypes—TNF receptor 1 (TNFR1), TNFR2, and herpes virus entry mediator (HVEM)—to exert various biological functions. TNFR1 induces an anti-tumor effect and Peyer's patch development, whereas TNFR2 is essential for immune responses against bacteria and viruses [1]. Human LTα and TNF that bind to murine TNFR1, but not to murine TNFR2, are not lethal in healthy mice except at extremely high doses, suggesting that LTα and TNF α exhibit their lethal side effects *via* TNFR2 [10,11]. Therefore, LTα as a cancer immunotherapeutic agent, a LTα mutant with selectively increased TNFR1-mediated bioactivity is needed. Previously, we successfully created a TNFR1-selective LTα mutant whose bioactivity *via* TNFR1 was several times that of wtLTα, and whose bioactivity *via* TNFR2 was 2.5% that of wtLTα [12]. However, to enhance therapeutic efficacy and suppress the side effect of LTα, it is necessary to create a LTα mutant with greatly increased TNFR1-mediated bioactivity and TNFR1-selectivity.

In this study, we attempted to create LTα mutants with selectively increased TNFR1-mediated bioactivity by using a phage display technique. We succeeded in creating a LTα mutant that had a much higher bioactivity *via* TNFR1 and an augmented affinity to TNFR1 compared with that of wtLTα, and demonstrated that this was due to the slow dissociation rate of the LTα mutant-TNFR1 complex. In addition, we showed that the LTα mutant differed from wtLTα by its ability to strongly and rapidly activate caspases. In contrast, the LTα mutant and wtLTα were similar to each other in their degree of activation of nuclear factor-kappa B (NFκB). Our findings suggest that this LTα mutant would be a superior candidate for a cancer immunotherapeutic agent.

2. Materials and methods

2.1. Cells

HEp-2 cells, a human carcinoma cell line derived via HeLa contamination, were purchased from the American Type Culture Collection (Manassas, VA), and cultured in RPMI 1640 medium (Wako Pure Chemical Industries, Osaka, Japan) supplemented with 10% fetal bovine serum (FBS), 1 mM sodium pyruvate, 50 μM 2-mercaptoethanol, and antibiotics. HT29.14S cells, a TNF/LT-sensitive subclone of HT29 human colon adenocarcinoma, were kindly provided by Dr. Carl Ware (La Jolla Institute for Allergy and Immunology, CA) [13]. HT29.14S cells were cultured in Dulbecco's Modified Eagle's Medium (Wako Pure Chemical Industries) supplemented with 10% FBS, 10 mM HEPES, and antibiotics. hTNFR2/mFas-PA cells are preadipocytes derived from TNFR1$^{-/-}$ TNFR2$^{-/-}$ mice expressing a chimeric receptor composed of the extracellular and transmembrane domain of human TNFR2 and the intracellular domain of mouse Fas, which is a member of the TNF receptor superfamily [14]; these cells were cultured in RPMI 1640 medium supplemented with 10% FBS, 5 μg/mL Blasticidin S HCl (Invitrogen, Carlsbad, CA), and antibiotics. MCF-7 cells were provided from the Institute of Development, Aging and Cancer, Tohoku University, and were cultured in Eagle's Minimum Essential Medium (Wako Pure Chemical Industries) supplemented with 10% FBS, 0.01 mg/mL bovine insulin, and antibiotics.

2.2. Construction of a library of lysine-deficient mutants of LTα

The phagemid vector pY03′, which encodes human wtLTα with the C-terminus of wtLTα fused to the N-terminus of the M13 phage g3p, was used as a PCR template for constructing a DNA library of lysine-deficient mutants of LTα. We performed a two-step PCR amplification using oligonucleotides containing the sequence NNS (where N represents A, C, G, or T; and S represents C or G) at Lys19, Lys28, Lys39, Lys84, Lys89, and Lys119 of wtLTα; the sequence NNS encodes all 20 standard amino acids. The products from the second PCR were digested with *NcoI* and *PstI* and then ligated into pY03′. The phagemid was electroporated into *Escherichia coli* (*E. coli*) TG1 cells (Stratagene, Cedar Creek, TX), yielding 2×10^6 independent clones. The phage library displaying lysine-deficient LTα molecules was prepared as described previously [12]. Briefly, pY03′-transformed TG1 cells were infected with M13KO7 helper phage (Invitrogen) and cultured for 6 h at 25 °C. The resultant phage particles were precipitated from the culture supernatant by using PEG (MP Biomedicals, Solon, OH) and suspended in NTE (100 mM NaCl, 10 mM Tris, 1 mM EDTA).

2.3. Selection of bioactive LTα mutants

Screening for bioactive LTα mutants was performed as described previously [12]. Briefly, an immunoplate was coated with soluble human TNFR1 (R&D Systems, Minneapolis, MN), and the prepared phage library was allowed to bind to the immobilized TNFR1. After a second round of panning, single colonies were picked and cultured. The resulting phage-containing culture supernatant was used for screening by enzyme-linked immunosorbent assay (ELISA) against human TNFR1.

2.4. Expression and purification of recombinant LTαs

pET15b plasmids (Novagen, Darmstadt, Germany) encoding LTαs were prepared and used to transform *E. coli* BL21(DE3) cells (Stratagene) for the expression of recombinant protein, as described previously [12]. Expression was induced by adding 1 mM isopropyl β-D-1-thiogalactopyranoside and incubating the cells at 37 °C for 6 h in Terrific Broth (Invitrogen Corporation, Carlsbad, CA) containing 0.4% glucose, 1.68 mM $MgSO_4$, and 100 μg/mL of ampicillin; all products were accumulated as inclusion bodies. The resultant inclusion bodies were washed, solubilized, reduced, and refolded by the methods previously described [12]. After dialysis against a buffer containing 20 mM Tris–HCl (pH 7.4) and 100 mM urea, active trimeric LTα proteins were purified by using a HiLoad Superdex 200PG column (GE Healthcare, UK) equilibrated with phosphate-buffered saline (pH 7.4) followed by ion-exchange chromatography (SP Sepharose Fast Flow for wtLTα; Q Sepharose Fast Flow for mutants of LTα); both columns were obtained from GE Healthcare. To create point mutants, we used pET15b-human wtLTα as a template with a KOD-plus mutagenesis kit (Toyobo, Osaka, Japan) according to the manufacturer's instructions. Recombinant point mutants were produced and purified as described earlier; SP Sepharose Fast Flow was used as the ion-exchange column. Protein concentration was measured by using Coomassie Protein Assay Reagent (Thermo Fisher Scientific, Rockford, IL). Sodium dodecyl sulfate–polyacrylamidegel electrophoresis (SDS–PAGE) analysis of LTαs was conducted under reducing conditions, and the proteins in the gels were stained with Coomassie brilliant blue. The electrostatic potential surface was generated by using GRASP software [15]. The electrostatic potential ranged from −7.5 kT to 7.5 kT. The relative accessible surface areas were calculated by using JOY software [16].

2.5. Cytotoxicity assays

HEp-2 cells were seeded at 4×10^4 cells per well in 96-well plates and incubated for 18 h with serially-diluted LTαs in the presence of 50 μg/mL cycloheximide. For the functional blocking assay, HEp-2 cells were treated with serially-diluted MAB225 (R&D Systems), an anti-TNFR1 antibody, for 30 min. The cells were then incubated with 100 ng/mL wtLTα and LTα mutants for 18 h in the presence of 50 μg/mL cycloheximide. For the caspase inhibition assay, HEp-2 cells were incubated with serially-diluted wtLTα or LTα mutants in the presence of 50 μg/mL cycloheximide and 50 mM zVAD-fmk (Calbiochem, Darmstadt, Germany) for 18 h. R2/Fas preadipocyte cells were seeded at 1.5×10^4 cells per well in 96-well plates and incubated for 48 h with serially-diluted LTαs in the presence of 50 μg/mL cycloheximide. The cytotoxicities of LTαs against HEp-2 cells and R2/Fas preadipocyte cells were assessed by using the standard methylene blue assay method as previously described [12]. HT29.14S and MCF-7 cells were seeded at 5×10^3 cells per well and incubated with LTαs in the presence of 80 U/mL human Interferon γ (IFNγ) (R&D Systems) for 72 h. After incubation, cell viability was measured by using a WST-8 assay kit (Nacalai Tesque, Kyoto, Japan) according to the manufacturer's instructions. The ratio of TNFR1-/TNFR2-mediated bioactivity was calculated as follows: activity of LTαs in HEp-2 cells/activity of LTαs in R2/Fas preadipocyte cells. The TNFR1/TNFR2 ratio for wtLTα was set equal to 1.

2.6. Analysis of binding kinetics by surface plasmon resonance

The binding kinetics of LTαs were analyzed and compared by using a surface plasmon resonance (SPR) method (BIAcore 2000, GE Healthcare, UK). Human TNFR1, TNFR2, or HVEM Fc chimera (R&D Systems, Inc.) was diluted to 50 μg/mL in 10 mM sodium acetate (pH 4.5) and immobilized onto a CM5 sensor chip by using an amine coupling kit (GE Healthcare, UK) as described previously [12]. During the association phase, wtLTα or LTα mutants diluted in HBS-EP running buffer (GE, Healthcare UK) to 37, 18.5, 9.3, 4.6, or 2.3 nM were passed over the immobilized TNFRs for 2 min at a flow rate 20 μL/min. During the dissociation phase, HBS-EP was run over the sensor chip for 1 min at a flow rate 20 μ L/min. Complexes were eluted by using 20 μL of 10 mM glycine–HCl (pH 2.0). Data were evaluated by using BIAevaluation 4.1 software (GE Healthcare UK) to apply a 1:1 Langmuir binding model. The obtained sensorgrams were fitted globally over the range of injected concentrations and simultaneously over the association and dissociation phases.

2.7. Evaluation of caspase-3/7 and -8 activities

HEp-2 cells were seeded at 4×10^4 cells per well in 96-well plates and then incubated for 6, 12, or 18 h with 10 ng/mL of the relevant LTα in the presence of 50 μg/mL cycloheximide. Activities of intracellular caspase-8 and caspase-3/7 were measured by using Caspase-Glo assays (Promega, Madison, WI) according to the manufacturer's instructions.

2.8. Evaluation of NFκB activities

HEp-2 cells were co-transfected with pGL4.32, a NFκB-responsive firefly luciferase expression vector, and pRL-TK, a thymidine kinase–regulated renilla luciferase expression vector (Promega) at a ratio of 90:1 for 18 h. The cells were then treated with 10 ng/mL of wtLTα or LTα mutants for 1, 2, 4, 6, 12, and 24 h. Expression levels of intracellular firefly luciferase and renilla luciferase were then measured by using the Dual-Luciferase Reporter Assay System (Promega). The expression level of firefly luciferase was normalized against that of renilla luciferase.

3. Results

3.1. Production of a highly bioactive LTα mutant

Our recent study showed that site-specific PEGylation of a lysine-deficient mutant of LTα might be useful for cancer therapy, because the mutant retained bioactivity after PEGylation [9]. Here, we attempted to create a lysine-deficient mutant of LTα with augmented bioactivity *via* TNFR1 and TNFR1-selective bioactivity that could be used for site-specific PEGylation in the future. A phage library displaying LTα mutants with randomized sequences in place of all lysine codons was prepared. For the construction of the phage library, two-step PCR was used to replace the lysine codons randomly with an NNS sequence. As a result, we successfully constructed a library with 2×10^6 independent clones, and performed two rounds of panning against immobilized human TNFR1; phage clones were screened for binding affinity to TNFR1 by conducting an ELISA (data not shown). We obtained three LTα mutants (mutLT1, mutLT2, and mutLT3), which were putative lysine-deficient mutants of LTα. DNA sequencing analysis of the LTα mutants confirmed that all 6 lysine residues present in wtLTα were mutated to other amino acids (Table 1). To investigate the properties of the LTα mutants in detail, we prepared recombinant LTα mutant proteins by using an *E. coli* expression system, as previously described [12]. LTα mutants and wtLTα were expressed in *E. coli* and obtained through refolding of inclusion bodies. Purified LTα mutants displayed a molecular mass of 18 kDa by SDS–PAGE analysis (Fig. 1A), and a molecular mass of approximately 60 kDa by size exclusion chromatography (Fig. 1B), indicating that LTα mutants form homotrimeric complexes, as does wtLTα. The isoelectric points (pI) of mutLT1, mutLT2, and mutLT3 were 6.16, 6.16, and 6.00, respectively whereas that of wtLTα was 8.94 (Table 1). We also visually assessed the changes in the surface electrostatic potential values by using GRASP software (Fig. 1C). Because of their lack of lysine residues, LTα mutants had more negative areas on their surface than did wtLTα.

3.2. Bioactivities of LTα mutants

To assess the TNFR1-mediated bioactivity of LTα mutants, cytotoxicity assays using HEp-2 cells were performed (Fig. 2A). wtLTα and LTα mutants showed dose-dependent cytotoxicity, and the bioactivity of each LTα mutant was higher than that of wtLTα in the HEp-2 cells (Fig. 2A). The bioactivity of mutLT1 was especially high (31.8 times that of wtLTα; Table 2). Furthermore, we confirmed that the LTα-induced cytotoxicity was blocked by the anti-TNFR1 antibody in all cases (Fig. 2B). These results indicate that the LTα mutants possess higher TNFR1-mediated bioactivity than that displayed by wtLTα. To confirm that the higher bioactivity of the LTα mutants was not specific to HEp-2 cells, we examined the bio-

Table 1
Amino acid sequences and the isoelectric points of LTα mutants. The pI values of LTαs were calculated by using a program in the Expert Protein Analysis System proteomics server of the Swiss Institute of Bioinformatics (Basel, Switzerland).

	Residue position						pI
	19	28	39	84	89	119	
wtLTα	Lys	Lys	Lys	Lys	Lys	Lys	8.94
mutLT1	Asn	Gln	Asn	Ser	Leu	Gly	6.16
mutLT2	Asn	Gln	Ser	Thr	Val	Val	6.16
mutLT3	Asp	Gln	Ala	Thr	Thr	Ala	6.00

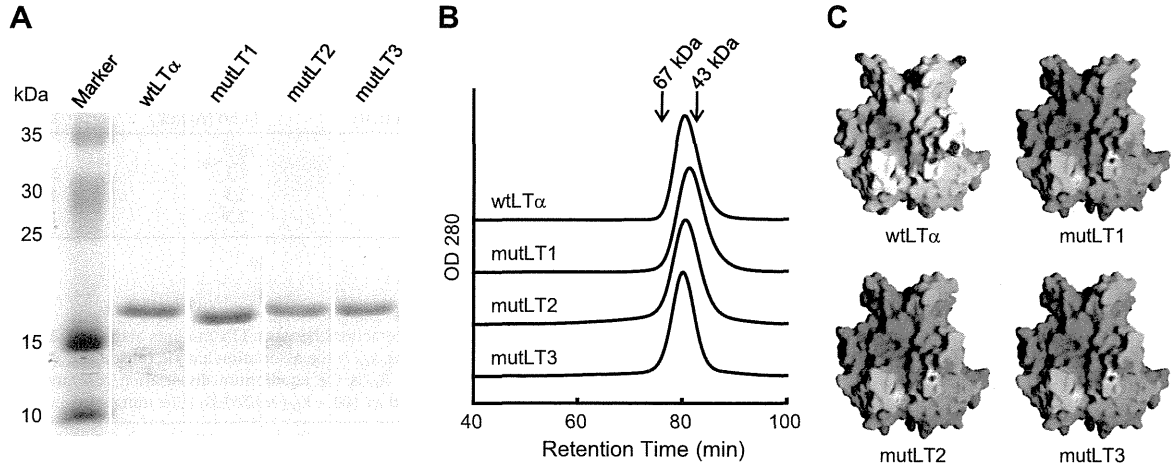

Fig. 1. Properties of recombinant LTα mutants. (A) SDS–PAGE analysis of wtLTα and LTα mutants. All products were separated on an SDS–PAGE gel and visualized by means of Coomassie Brilliant Blue staining. Marker indicates molecular weight standards. (B) Chromatograms of purified wtLTα and LTα mutants. wtLTα or LTα mutants were loaded onto a size-exclusion column and eluted at 1.0 mL/min. (C) The electrostatic potential surface was generated by using GRASP software. Red and blue indicate negative and positive electrostatic potentials, respectively. The electrostatic potential ranged from −7.5 kT (bright blue) to 7.5 kT (bright red). The relative accessible surface areas were calculated by using JOY software.

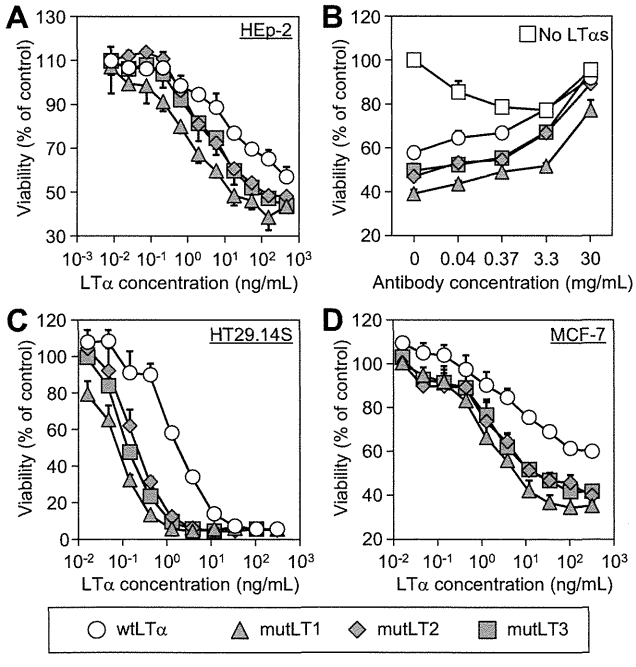

Fig. 2. TNFR1-mediated cytotoxic activity of wtLTα and LTα mutants. (A) HEp-2 cells were incubated with wtLTα or LTα mutants in the presence of cycloheximide. After 18 h incubation, cell viability was assessed by methylene blue assay. (B) HEp-2 cells were treated with serially-diluted MAB225, an anti-TNFR1 neutralizing antibody, for 30 min. The cells were then incubated with 100 ng/mL wtLTα or LTα mutants in the presence of cycloheximide. After 18 h incubation, the cell viability was assessed by methylene blue assay. (C) HT29.14S cells and (D) MCF-7 cells were incubated with wtLTα or LTα mutants in the presence of IFNγ. After 72 h incubation, the cell viability was assessed by WST-8 assay. EC30 and EC50 are the concentrations of LTα required for 30% and 50% inhibition of cell viability, respectively. Each value represents the mean ± SD ($n = 4$).

activities of mutLTαs in two other cell types (Fig. 2C and D, Table 2). When compared with wtLTα, the LTα mutants exhibited 8–24 times the cytotoxicity in HT29.14S cells, and 16–34 times the cytotoxicity in MCF-7 cells (Fig. 2C and D, Table 2). To specifically evaluate the TNFR2-mediated bioactivity of the LTα mutants, we examined the levels of cytotoxity induced by LTα mutants in hTNFR2/mFas-PA cells. These cells have been engineered to exhibit hTNFR2- but not hTNFR1-mediated activities [14]. The human TNFR2-mediated bioactivities of LTα mutants were 2.2–4.1 times those of wtLTα in hTNFR2/mFas-PA cells (Fig. 3). The calculated ratios of TNFR1-mediated bioactivity by using HEp-2 cells/TNFR2-mediated bioactivity induced by mutLT1, mutLT2, and mutLT3 were 7.8, 3.2, and 1.9 times that of wtLTα, respectively. This result suggests that LTα mutants, especially mutLT1, have selectivity for TNFR1 in addition to their augmented bioactivity.

Next, to measure the binding affinity of LTα mutants to TNFRs, we performed an SPR analysis by using a BIAcore 2000 biosensor (Table 3). The binding affinities of mutLT1, mutLT2 and mutLT3 to TNFR1 were 2.7, 2.0, and 1.4 times those of wtLTα, respectively. We considered that the increased affinity of LTα mutant for TNFR1 might be related to the enhanced bioactivity through this receptor. In particular, k_{off} values for LTα mutants binding to TNFR1 were 39–57% of the value for wtLTα, whereas the k_{on} values for LTα mutants binding to TNFR1 were almost the same as that for wtLTα. These results suggest that TNFR1 interacts more strongly with the LTα mutants than wtLTα due to slow dissociation kinetics, and that this binding mode between LTα mutant and TNFR1 induces a potent signaling pathway. We then evaluated the affinity of the LTα mutants for TNFR2 by using SPR methodology (Table 4). The affinity of TNFR2 for LTα mutants was 1.5–2.1 times that for wtLTα due to fast association kinetics. Taken together, these results indicate that the binding modes of LTα mutants to TNFR1 and TNFR2 might dictate their bioactivity.

We previously demonstrated that Lys84 in LTα plays a crucial role in the protein's interaction with the main chain of TNFR1 [12]. Therefore, to investigate the importance of the amino acid sequence at position 84, we created LTα mutants with Lys84 replaced by Ser84 (K84S), Thr84 (K84T), or Ala84 (K84A), and evaluated their binding kinetics and bioactivities *via* TNFR1. We found that these point mutants exhibited a slower dissociation rate and increased bioactivity *via* TNFR1 when compared with wtLTα. K84S showed especially high bioactivity even though its affinity for TNFR1 was lower than that of wtLTα (Table 5).

3.3. Activation of caspases by LTα mutant

It is known that TNFR1-mediated cell death is regulated by the activities of caspases including caspase-3, -7, and -8 [17].

Table 2
The TNFR1-mediated bioactivities of wtLTα and LTα mutants. EC30 and EC50 were calculated from the cytotoxic activity of wtLTα and LTα mutants against HEp-2, HT29.14S and MCF-7 cells. Relative activity values were calculated as EC30 (wtLTα)/EC30 (LTα mutant) or EC50 (wtLTα)/EC50 (LTα mutant).

	HEp-2 cells		HT29.14S cells		MCF-7 cells	
	EC30 (ng/mL)	Relative activity	EC50 (ng/mL)	Relative activity	EC50 (ng/mL)	Relative activity
wtLTα	47.7	1.0	1.80	1.0	36.7	1.0
mutLT1	1.5	31.8	0.08	23.6	1.1	33.7
mutLT2	6.8	7.0	0.21	8.5	2.3	16.0
mutLT3	7.8	6.1	0.13	14.2	2.3	16.0

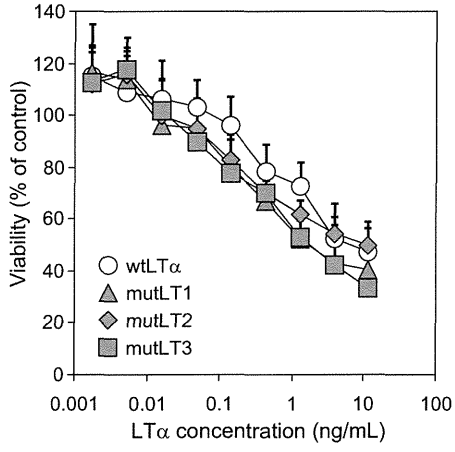

	EC30 (ng/mL)	Relative activity (% vs wtLTα)
wtLTα	1.39	100
mutLT1	0.34	409
mutLT2	0.64	217
mutLT3	0.43	323

Fig. 3. TNFR2-mediated cytotoxic activities of wtLTα and LTα mutants. hTNFR2/mFas-PA cells were incubated with serial dilutions of wtLTα or LTα mutants in the presence of cycloheximide. After 48 h incubation, cell viability was assessed by methylene blue assay. EC30 is the concentration of LTα required for 30% inhibition of cell viability. Each value represents the mean ± SD ($n = 4$).

Table 3
The binding kinetics of interactions between LTα mutants and hTNFR1 analyzed by using an SPR biosensor. k_{on} is the association kinetic constant; k_{off} is the dissociation kinetic constant; and K_D is the equilibrium dissociation constant. Relative affinity values were calculated as 100 × K_D (wtLTα)/K_D (LTα mutant).

	k_{on} (10^6/M s)	k_{off} (10^{-4}/s)	K_D (10^{-10}/M)	Relative affinity (% vs wtLTα)
wtLTα	1.2	6.1	4.9	100
mutLT1	1.3	2.4	1.8	269
mutLT2	1.4	3.5	2.5	195
mutLT3	0.97	3.4	3.4	143

Therefore, to examine the mechanism behind the augmentation of TNFR1-mediated bioactivity, we investigated the association between caspase activity and LTα mutant-induced cell death. First, we treated cells with LTα mutants in the presence of a broad caspase inhibitor, zVAD-fmk, and analyzed the cell viability (Fig. 4A). The results showed that zVAD-fmk almost completely abrogated the cytotoxicity induced by wtLTα and LTα mutants. These results indicate that both wild-type and LTα mutant-induced cell death were dependent on the activation of caspase. We then examined the activity of caspase-3/7 (Fig. 4B) and -8 (Fig. 4C) induced by LTα mutants in HEp-2 cells. LTα mutants, especially

Table 4
Binding kinetics of interactions between LTα mutants and hTNFR2 were analyzed by using an SPR biosensor. k_{on} is the association kinetic constant; k_{off} is the dissociation kinetic constant; and K_D is the equilibrium dissociation constant. Relative affinity values were calculated as 100 × K_D (wtLTα)/K_D (LTα mutant).

	k_{on} (10^6/M s)	k_{off} (10^{-4}/s)	K_D (10^{-10}/M)	Relative affinity (% vs wtLTα)
wtLTα	2.8	23.5	8.3	100
mutLT1	4.7	25.0	5.4	154
mutLT2	6.2	24.0	3.9	213
mutLT3	4.5	25.3	5.6	148

mutLT1, which has the highest bioactivity, quickly and strongly induced the activation of caspases. These results suggest that stabilization of the LTα -TNFR1 complex by the presence of LTα mutant contributed to increased caspase activity, which in turn induced cytotoxic effects.

3.4. Activation of NFκB by LTα mutants

It is well known that TNFR1 activates NFκB signaling pathway in addition to the caspase cascade [18,19]. Therefore, to investigate whether the LTα mutants activate NFκB, we assessed the association between NFκB activity and LTα mutant-induced cell death. First, we prepared cells transfected with luciferase expressing vector activated by NFκB. Then, we treated cells with LTα mutants and analyzed the NFκB activity by measuring the expression level of luciferase (Fig. 5). Despite the higher TNFR1-mediated bioactivity of LTα mutants, we found that NFκB activity was induced to a similar extent by LTα mutants and wtLTα. This finding indicates that the LTα mutants selectively activate the caspase cascade but not NFκB activation *via* TNFR1.

4. Discussion

When constructing a LTα mutant as an anti-cancer agent, it is important that the mutant exhibits TNFR1 selectivity because of the lethal side-effects of TNFR2-mediated bioactivity. We previously created a LTα mutant (R1selLT), which had only 2.5% of the TNFR2-mediated bioactivity of wtLTα and 3.5 times of the TNFR1-mediated bioactivity of wtLTα [12]. The ratio of TNFR1/TNFR2 bioactivity of R1selLT was 145.8 times that of wtLTα. In addition to TNFR1 selectivity, augmentation of TNFR1-mediated bioactivity is also highly desirable in a therapeutic agent for cancer. Here, we created three lysine-deficient LTα mutants with greatly increased levels of TNFR1-mediated bioactivity through an altered binding mode. These mutants showed preferentially augmented bioactivity *via* TNFR1 compared with TNFR2. The TNFR1 selectivity of mutLT1, 2, and 3 was 7.8, 3.2, and 1.9 times that of wtLTα, respectively. Although the TNFR1 selectivity was lower for mutLT1 than for R1selLT, the TNFR1-mediated bioactivity of mutLT1 was 31.8 times that of wtLTα compared to 3.5 times of R1selLT. Such extreme augmentation of bioactivity is rarely reported. As

Table 5
Binding kinetics of interactions between point-mutated LTαs and hTNFR1 were analyzed by using an SPR biosensor. k_{on} is the association kinetic constant; k_{off} is the dissociation kinetic constant; and K_D is the equilibrium dissociation constant. Relative affinity values were calculated as 100 × K_D (wtLTα)/K_D (point mutated LTα). TNFR1-mediated relative activities of LTα mutants were calculated from the concentration of LTα required for 30% inhibition of HEp-2 cell viability.

	k_{on} (10^6/M s)	k_{off} (10^{-4}/s)	K_D (10^{-10}/M)	Relative affinity (% vs wtLTα)	Relative activity(% vs wtLTα)
wtLTα	1.2	6.1	4.9	100	100
K84S	0.28	2.2	8.0	62	4810
K84T	1.0	4.3	118	195	1100
K84A	1.5	5.3	3.5	143	910

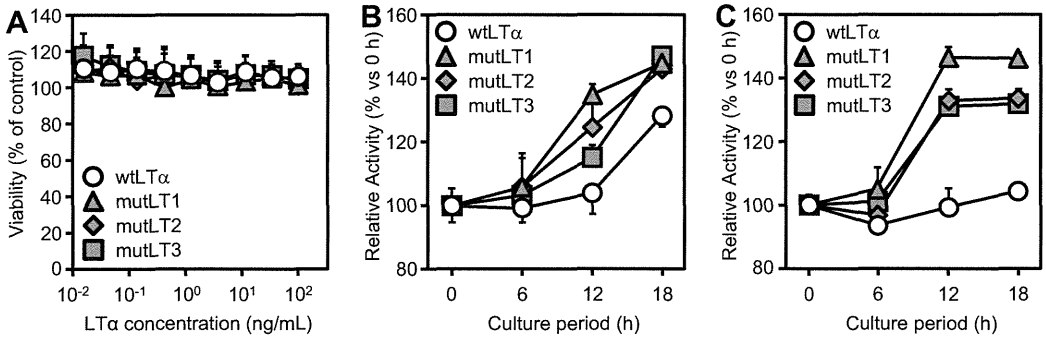

Fig. 4. Caspase activities in HEp-2 cells treated with wtLTα or LTα mutants. (A) Cycloheximide treated HEp-2 cells were incubated with wtLTα or LTα mutants in the presence of zVAD-fmk. After 18 h incubation, cell viability was assessed by methylene blue assay. (B and C) Cycloheximide treated HEp-2 cells were incubated for 6, 12, or 18 h with 10 ng/mL LTαs, and the activities of intracellular caspase-3/7 (B) and intracellular caspase-8 (C) were measured by using Caspase-Glo assays. Each value represents the mean ± SD (n = 4).

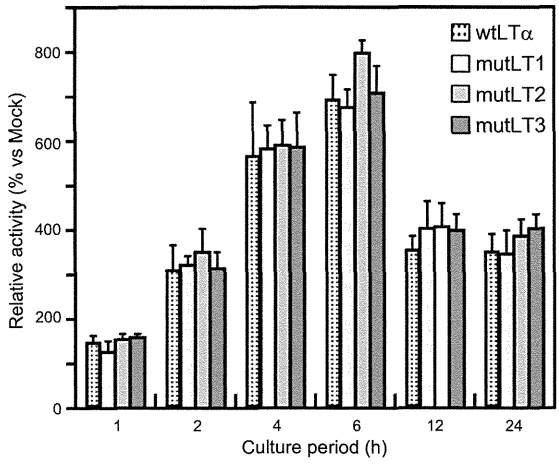

Fig. 5. NFκB activities in HEp-2 cells treated with wtLTα or LTα mutants. HEp-2 cells were co-transfected with pGL4.32 and pRL-TK (Promega). Eighteen hours after transfection, the cells were treated with 10 ng/mL LTαs for the indicated period. The intracellular luciferase activity was then quantified. Data are shown as the relative NFκB activity compared with the mock-transfected group. Each bar represents the mean ± SD (n = 4).

described above, high TNFR1 selectivity of R1selLT was mainly resulted from the significant decreased TNFR2-mediated bioactivity. On the other hand, the TNFR1 selectivity of mutLT1 was obtained from the augmented TNFR1-mediated bioactivity, while TNFR2-mediated bioactivity was maintained. On this point, TNFR2 is known to play essential role for the induction of immune responses. Therefore, we consider that a TNFR1-selective LTα mutants with high TNFR1-mediated and equivalent TNFR2-mediated bioactivity compared to wtLTα, such as mutLT1, would be a superior candidate for cancer therapy by combination of direct pro-apoptotic effects of LTα on tumor cells and an enhancement of local/systemic immunity.

Many cellular signaling processes are hypothesized to depend not only on the equilibrium strength of the ligand–receptor interactions but also on the average durations or kinetic dissociation rates of these interactions [20–23]. In some cases, the intensity of distal signaling depends on the off-rate rather than on the on-rate of the ligand–receptor complex [20,22]. For interactions with TNFR1, the LTα mutants exhibited higher k_{off} values compared with the value for wtLTα, whereas the k_{on} values for the LTα mutants were almost same as that for wtLTα. In addition, the bioactivity of wtLTα and LTα mutants was related to k_{off} but not to k_{on}. These data suggest that the LTα mutants interact with TNFR1 by slow dissociation and induce robust signal transduction. In contrast, for interactions with TNFR2, the LTα mutants showed a higher k_{on} than that for wtLTα, whereas the k_{off} values for the LTα mutants was almost same as that for wtLTα. These data indicate that the detailed molecular dissection of ligand-receptor binding kinetics is important for the construction of functional LTα mutants with desired TNFR-mediated bioactivity.

We previously demonstrated that Lys84 of LTα plays a crucial role in the protein's interaction with the main chain of TNFR1 [12]. Here, to explore the role of Lys84 further, we created LTα mutants with Lys84 replaced by Ser84 or Thr84, and found that the mutant with Ser84 showed slower dissociation kinetics and increased bioactivity when compared with wtLTα or the other mutants (Table 5). These results suggest that Lys84 contributes to the TNFR1-mediated bioactivity and the binding kinetics of the TNFR1–LTα interaction. In all three mutants analyzed here, the amino acid Lys at position 28 was changed to Gln (Table 1). Whereas these mutants exhibited increased TNFR1-mediated bioactivity, our previous data showed that a mutant with a K28Q substitution had decreased TNFR1-mediated bioactivity compared with that of wtLTα. Furthermore, mutLT2, which has the Lys at position 39 replaced by Ser, showed slightly increased TNFR2-mediated bioactivity, but a mutant containing the equivalent substitution at the same position showed decreased TNFR2-mediated bioactivity in our previous study [12]. These results suggest

that the sum of the mutations, including those at positions 28 and 39, were responsible for the augmented binding affinities to TNFR1 and TNFR2.

TNFR1 triggers apoptotic caspase signaling following activation of Fas-associated protein with death domain (FADD) [17]. At the same time, triggering of TNFR1 signals induces the anti-apoptotic NFκB cascade following the activation of TNF receptor-associated death domain (TRADD) and TNF receptor-associated factor (TRAF) adaptors [18,19,24]. Active NFκB induces transcription of a set of genes encoding anti-apoptotic proteins [25,26]. Therefore, in many cell types, TNF α has no apoptotic effects due to the parallel triggering by TNF α of a signaling pathway that activates NFκB *via* the TRADD and TRAF adaptors. Here, however, we found that the LTα mutants, which showed augmented bioactivity *via* TNFR1, efficiently induced caspase activation but induced NFκB to the same level as that induced by wtLTα (Figs. 4 and 5). We consider that the slower rate of dissociation of the LTα mutants from TNFR1 was important to the activation of FADD signaling cascade, but not to the activation of TRADD and TRAF adaptors. We speculate that the alteration of the binding mode of LTα mutant to TNFR1 increased the caspase signaling pathway, but not TRADD- and TRAF-mediated NFκB signaling. These findings will facilitate the construction of functional LTα mutants with even higher receptor selectivity and bioactivity in the future.

5. Conclusions

Here, we created highly bioactive LTα mutants with TNFR1-selectivity by using a phage display technique, and we clarified the molecular basis of their augmented TNFR1-mediated bioactivity. A better understanding of the correlation between structure, kinetic behavior, and activity will likely accelerate drug discovery because it will increase awareness of the properties of therapeutic proteins. We suggest that LTα mutants have the potential to be a powerful tool for cancer therapy by combination of direct pro-apoptotic effects of LTα on tumor cells and an enhancement of local/systemic immunity, and that our findings provide valuable information for the construction of even more functional LTα mutants.

Acknowledgements

The authors declare that they have no conflict of interests. This study was supported in part by grants from the Ministry of Health, Labor, and Welfare in Japan; by the Research on Health Sciences focusing on Drug Innovation from the Japan Health Sciences Foundation; and by the Takeda Science Foundation.

References

[1] Neumann B, Luz A, Pfeffer K, Holzmann B. Defective Peyer's patch organogenesis in mice lacking the 55-kD receptor for tumor necrosis factor. J Exp Med 1996;184:259–64.
[2] Kratz A, Campos-Neto A, Hanson MS, Ruddle NH. Chronic inflammation caused by lymphotoxin is lymphoid neogenesis. J Exp Med 1996;183:1461–72.
[3] Koni PA, Sacca R, Lawton P, Browning JL, Ruddle NH, Flavell RA. Distinct roles in lymphoid organogenesis for lymphotoxins alpha and beta revealed in lymphotoxin beta-deficient mice. Immunity 1997;6:491–500.
[4] Schrama D, thor Straten P, Fischer WH, McLellan AD, Brocker EB, Reisfeld RA, et al. Targeting of lymphotoxin-alpha to the tumor elicits an efficient immune response associated with induction of peripheral lymphoid-like tissue. Immunity 2001;14:111–21.
[5] Schrama D, Voigt H, Eggert AO, Xiang R, Zhou H, Schumacher TN, et al. Immunological tumor destruction in a murine melanoma model by targeted LTalpha independent of secondary lymphoid tissue. Cancer Immunol Immunother 2008;57:85–95.
[6] Ryan SM, Mantovani G, Wang X, Haddleton DM, Brayden DJ. Advances in PEGylation of important biotech molecules: delivery aspects. Expert Opin Drug Deliv 2008;5:371–83.
[7] Yamamoto Y, Tsutsumi Y, Yoshioka Y, Nishibata T, Kobayashi K, Okamoto T, et al. Site-specific PEGylation of a lysine-deficient TNF-alpha with full bioactivity. Nat Biotechnol 2003;21:546–52.
[8] Shibata H, Yoshioka Y, Ikemizu S, Kobayashi K, Yamamoto Y, Mukai Y, et al. Functionalization of tumor necrosis factor-alpha using phage display technique and PEGylation improves its antitumor therapeutic window. Clin Cancer Res 2004;10:8293–300.
[9] Narimatsu S, Yoshioka Y, Watanabe H, Masano T, Morishige T, Yao X, et al. Lysine-deficient lymphotoxin-alpha mutant for site-specific PEGylation. Cytokine 2011;56:489–93.
[10] Everaerdt B, Brouckaert P, Shaw A, Fiers W. Four different interleukin-1 species sensitize to the lethal action of tumour necrosis factor. Biochem Biophys Res Commun 1989;163:378–85.
[11] Brouckaert P, Libert C, Everaerdt B, Fiers W. Selective species specificity of tumor necrosis factor for toxicity in the mouse. Lymphokine Cytokine Res 1992;11:193–6.
[12] Yoshioka Y, Watanabe H, Morishige T, Yao X, Ikemizu S, Nagao C, et al. Creation of lysine-deficient mutant lymphotoxin-alpha with receptor selectivity by using a phage display system. Biomaterials 2010;31:1935–43.
[13] Browning JL, Miatkowski K, Sizing I, Griffiths D, Zafari M, Benjamin CD, et al. Signaling through the lymphotoxin beta receptor induces the death of some adenocarcinoma tumor lines. J Exp Med 1996;183:867–78.
[14] Abe Y, Yoshikawa T, Kamada H, Shibata H, Nomura T, Minowa K, et al. Simple and highly sensitive assay system for TNFR2-mediated soluble- and transmembrane-TNF activity. J Immunol Methods 2008;335:71–8.
[15] Nicholls A, Sharp KA, Honig B. Protein folding and association: insights from the interfacial and thermodynamic properties of hydrocarbons. Proteins 1991;11:281–96.
[16] Mizuguchi K, Deane CM, Blundell TL, Johnson MS, Overington JP. JOY: protein sequence-structure representation and analysis. Bioinformatics 1998;14:617–23.
[17] Sheikh MS, Huang Y. Death receptor activation complexes: it takes two to activate TNF receptor 1. Cell Cycle 2003;2:550–2.
[18] Chen G, Goeddel DV. TNF-R1 signaling: a beautiful pathway. Science 2002;296:1634–5.
[19] Magne N, Toillon RA, Bottero V, Didelot C, Houtte PV, Gerard JP, et al. NF-kappaB modulation and ionizing radiation: mechanisms and future directions for cancer treatment. Cancer Lett 2006;231:158–68.
[20] Hlavacek WS, Redondo A, Metzger H, Wofsy C, Goldstein B. Kinetic proofreading models for cell signaling predict ways to escape kinetic proofreading. Proc Nat Acad Sci USA 2001;98:7295–300.
[21] Liu ZJ, Haleem-Smith H, Chen H, Metzger H. Unexpected signals in a system subject to kinetic proofreading. Proc Nat Acad Sci USA 2001;98:7289–94.
[22] Krippner-Heidenreich A, Tubing F, Bryde S, Willi S, Zimmermann G, Scheurich P. Control of receptor-induced signaling complex formation by the kinetics of ligand/receptor interaction. J Biol Chem 2002;277:44155–63.
[23] Torigoe C, Faeder JR, Oliver JM, Goldstein B. Kinetic proofreading of ligand–FcepsilonRI interactions may persist beyond LAT phosphorylation. J Immunol 2007;178:3530–5.
[24] Kim JY, Lee JY, Kim DG, Koo GB, Yu JW, Kim YS. TRADD is critical for resistance to TRAIL-induced cell death through NF-kappaB activation. FEBS Lett 2011;585:2144–50.
[25] Arch RH, Gedrich RW, Thompson CB. Tumor necrosis factor receptor-associated factors (TRAFs) – a family of adapter proteins that regulates life and death. Genes Dev 1998;12:2821–30.
[26] Deveraux QL, Reed JC. IAP family proteins–suppressors of apoptosis. Genes Dev 1999;13:239–52.

Neuroscience Letters 534 (2013) 85–89

Contents lists available at SciVerse ScienceDirect

Neuroscience Letters

journal homepage: www.elsevier.com/locate/neulet

Proteomic analysis of the hippocampus in Alzheimer's disease model mice by using two-dimensional fluorescence difference in gel electrophoresis

Masaoki Takano[a], Takuya Yamashita[b,c], Kazuya Nagano[c], Mieko Otani[a], Kouji Maekura[a], Haruhiko Kamada[c], Shin-ichi Tsunoda[c], Yasuo Tsutsumi[b,c], Takami Tomiyama[e,f], Hiroshi Mori[e,f], Kenji Matsuura[d], Shogo Matsuyama[d,*]

[a] Laboratory of Molecular Cellular Biology, School of Pharmaceutical Sciences, Kobe Gakuin University, 1-1-3 Minatojima, Chuo-ku, Kobe 650-8586, Japan
[b] Laboratory of Toxicology and Safety Science, Graduate School of Pharmaceutical Sciences, Osaka University, 1-6 Yamadaoka, Suita, Osaka 565-0871, Japan
[c] Laboratory of Biopharmaceutical Research, National Institute of Biomedical Innovation, 7-6-8 Saito-Asagi, Ibaraki, Osaka 567-0085, Japan
[d] Faculty of Pharmaceutical Sciences, Himeji Dokkyo University, 7-2-1 Kamiohno, Himeji 670-8524, Japan
[e] Department of Neuroscience, Osaka City University Graduate School of Medicine, Osaka 545-8585, Japan
[f] Core Research for Evolutional Science and Technology, Japan Science and Technology Agency, Japan

HIGHLIGHTS

- We perform the proteome for $APP_{E693\Delta}$-transgenic mice. Methods are two-dimensional fluorescence difference in gel electrophoresis and mass spectrometry techniques. The expression of 14 proteins are changed in the brain. Aβ oligomers contribute to the expression of proteins.

ARTICLE INFO

Article history:
Received 4 August 2012
Received in revised form 13 October 2012
Accepted 6 November 2012

Keywords:
Proteome
Amyloid β oligomers
Alzheimer's disease
Hippocampus
2D-DIGE

ABSTRACT

We previously identified the E693Δ mutation in amyloid precursor protein (APP) in patients with Alzheimer's disease (AD) and then generated APP-transgenic mice expressing this mutation. As these mice possessed abundant Aβ oligomers from 8 months of age but no amyloid plaques even at 24 months of age, they are a good model to study pathological effects of amyloid β (Aβ) oligomers. The two-dimensional fluorescence difference in gel electrophoresis (2D-DIGE) technology, using a mixed-sample internal standard, is now recognized as an accurate method to determine and quantify proteins. In this study, we examined the proteins for which levels were altered in the hippocampus of 12-month-old $APP_{E693\Delta}$-transgenic mice using 2D-DIGE and liquid chromatography–tandem mass spectrometry (LC–MS/MS). Fourteen proteins were significantly changed in the hippocampus of $APP_{E693\Delta}$-transgenic mice. Actin cytoplasmic 1 (β-actin), heat shock cognate 71 kDa, γ-enolase, ATP synthase subunit β, tubulin β-2A chain, clathrin light chain B (clathrin) and dynamin-1 were increased. Heat shock-related 70 kDa protein 2, neurofilament light polypeptide (NFL), stress-induced-phosphoprotein 2, 60 kDa heat shock protein (HSP60), α-internexin, protein kinase C and casein kinase substrate in neurons protein 1 (Pacsin 1), α-enolase and β-actin were decreased. Western blotting also validated the changed levels of HSP60, NFL, clathrin and Pacsin 1 in $APP_{E693\Delta}$-transgenic mice. The identified proteins could be classified as cytoskeleton, chaperons, neurotransmission, energy supply and signal transduction. Thus, proteomics by 2D-DIGE and LC–MS/MS has provided knowledge of the levels of proteins in the early stages of AD brain.

1. Introduction

AD is neuropathologically characterized by abnormal accumulation of extracellular amyloid plaques and intracellular neurofibrillary tangles throughout cortical and limbic regions. Although the current amyloid cascade hypothesis [6] and tau hypothesis [15] provide frameworks for studying AD pathogenesis. Recently, diverse lines of evidence suggest that Aβ peptides play more important roles in AD pathogenesis [13,16,20]. Especially, soluble oligomers of Aβ could be a cause of synaptic and cognitive dysfunction in the early stages of AD. To address the relationship between Aβ oligomers and pathological features of AD, we generated APP transgenic mice expressing the E693Δ mutation, which enhanced Aβ oligomerization without fibrillization [25]. It might provide a clue for elucidating AD pathology caused by Aβ oligomers to analyze the $APP_{E693\Delta}$-transgenic mice.

* Corresponding author. Tel.: +81 79 223 6849; fax: +81 79 223 6857.
E-mail address: shogo@himeji-du.ac.jp (S. Matsuyama).

0304-3940/$ – see front matter © 2012 Elsevier Ireland Ltd. All rights reserved.
http://dx.doi.org/10.1016/j.neulet.2012.11.010

One of the most utilized approaches in proteomics to quantify and identify proteins is two dimensional gel electrophoresis (2DE) and mass spectrometry (MS) [5]. Proteomic approaches were most widely based on methods using differential expression on 2D-PAGE gels, or more recently 2D chromatography, followed by mass spectrometry protein identification. Compared to these conventional analyses, 2D-DIGE has higher reproducibility and sensitivity because of its internal standard design which minimizes gel-to-gel variation, improves spot matching, reduces number of gels needed, and permits quantitative analysis of small sample amounts.

In this study, we studied the altered expression of proteins in the hippocampus of $APP_{E693\Delta}$-transgenic mice using 2D-DIGE and LC–MS/MS approach. This approach revealed that the levels of at least 14 proteins were altered in the hippocampus of 12-month-old $APP_{E693\Delta}$-transgenic mice. These findings suggest that Aβ oligomers might cause synaptic and cognitive dysfunction by affecting the expression of these proteins in the hippocampus.

2. Experimental procedures

2.1. Materials

Sodium dodecyl sulfate, urea, thiourea, CHAPS, dithiothreitol, iodoacetamide, bromophenol blue, and RNase A and DNase I for SDS-PAGE or 2DE were all obtained from Wako Pure Chemical Industries (Osaka, Japan). Source information for all other assay reagents and materials are incorporated into their respective assay methods described below.

2.2. Animal subjects

Transgenic mice expressing human APP_{695} with the APP E693Δ mutation under the mouse prion promoter were used [25]. Heterozygous human $APP_{E693\Delta}$-transgenic mice and age-matched non-transgenic littermates were sacrificed at 12 months of age, and their hippocampi were isolated on an ice-cold plate. Animal care and handling were performed strictly in accordance with the Guidelines for Animal Experimentation at Kobe Gakuin University and Himeji Dokkyo University. Every effort was made to minimize the number of animals used and their suffering.

2.3. Protein labeling with CyDyes

Equal amounts of total protein from 4 hippocampi of $APP_{E693\Delta}$-transgenic mice or age-matched non-transgenic littermates were separately pooled. Protein samples were labeled with CyDyes (GE Healthcare, Piscataway, NJ), as per manufacturer's instructions. In brief, 50 μg of total protein from each sample was mixed in a tube and labeled with Cy2 minimal dye, and 50 μg protein taken from the mix was used as an internal standard on each gel for the three subsequent 2DE and image analysis. In parallel, 50 μg protein from each sample was labeled with either Cy3 or Cy5, and the dyes scrambled within each group to avoid possible dye bias. As a result, one replicate was Cy3 labeled proteins and another replicate was Cy5 labeled proteins. Two replicates (Cy3 and Cy5 labeled samples) were mixed, divided and applied each three independent gels. The sample volumes were adjusted to 18 μL with labeling buffer (7M urea, 2 M thiourea, 4% CHAPS, 30 mM Tris), followed by addition of 1 μL dye (working solution) to each individual sample. The samples were left on ice for 30 min in the dark, followed by adding 1 μL of 10 mmol/L lysine to stop the reaction.

2.4. 2D electrophoresis and image analysis

One sample from each of the CyDye groups was mixed together and adjusted to final concentrations of 1% DTT, 1% IPG buffer at a total volume of 350 μL with lysis buffer (7 M urea, 2 M thiourea, 4% CHAPS) and was used to 24 cm pH 4–7 IPG strips (non-linear; GE Healthcare, Piscataway, NJ) overnight. First dimension isoelectric focusing (IEF) was carried out with IPGphor II (GE Healthcare, Piscataway, NJ). Second dimension SDS-PAGE was performed by mounting the IPG strips onto 20 × 26 cm 12.5% DIGE gels (GE Healthcare, Piscataway, NJ) using Ettan DALT six Large Electrophoresis System (GE Healthcare, Piscataway, NJ) and running the gels at 16 mA/gel for the initial hour and 25 mA/gel at 25 °C constantly until bromophenol blue reached the bottom of the gel. The lysates were labeled at the ratio of 50 μg proteins: 400 pmol Cy3 or Cy5 protein-labeling dye (GE HealthcareBiosciences) in dimethylformamide according to the manufacturer's protocol.

In summary, three analytical gels were completed in total, running 25 μg of pooled reference sample labeled with Cy2, along with two samples (25 μg each), one labeled with Cy3 and the other labeled with Cy5. Gels selected for picking were stained with Deep purple (GE Healthcare, Piscataway, NJ). Approximately 1100 spots were matched across all three analytical gels. The analytical gel was picked using an automated robotic system, Ettan Spot picker (GE Healthcare, Piscataway, NJ). The pick list was created based on the Deep purple image. 2 mm gel plugs were picked, washed, reduced and alkylated, and then digested with trypsin, and the resulting peptides were extracted. Gel trypsinization was performed as previously described [24].

2.5. LC/MS/MS identification

Trypsinized peptides were analyzed by nano LC/MS/MS on a ThermoFisher LTQ Orbitrap XL. In brief, 30 mL of hydrolysate was loaded onto a 5 mm 675 mm ID C12 (Jupiter Proteo, Phenomenex) vented column at a flow-rate of 10 mL/min. Gradient elution was conducted on a 15 cm by 75 mm ID C12 column at 300 nL/min. A 30 min gradient was employed. The mass spectrometer was operated in a data-dependent mode, and the six most abundant ions were selected for MS/MS. Mass spectrometry results were searched using Mascot (www.matrixscience.com). Samples were processed in the Scaffold algorithm using DAT files generated by Mascot. Parameters for LTQ Orbitrap XL data require a minimum of two peptide matches per protein with minimum probabilities of 90% at the protein level.

2.6. Western blotting

Approximately 25 μg of protein from mouse hippocampus was applied to a 12.5% acrylamide gel and SDS-polyacrylamide gel electrophoresis was performed at 17.5 mA/gel for 2 h in second dimension. The gels were transferred onto PVDF membranes (Pall Corporation, Pensacola, FL, USA), in a trans-blot electrophoresis transfer cell (Nihon Eido, Tokyo, Japan). Western blotting was performed by using monoclonal antibodies against β-actin (diluted 1:1000, Cell Signaling, USA) and clathrin (diluted 1:250, Abcam, USA), polyclonal antibodies HSP60, NFL, voltage-dependent anion-selective channel protein 1 (VDAC) (diluted 1:1000, Cell Signaling, USA) and Pacsin 1 (diluted 1:500, Millipore, USA). Peroxidase-conjugated antibody (diluted 1:5000, Abcam, USA) was used as secondary antibody. The reaction was detected by chemiluminescence with ECL reagents (Pierce Biotechnology, USA). A semi quantitative analysis based on optical density was performed by ImageJ software (available at http://www.rsbweb.nih.gov/ij).

3. Results and discussion

The 2D-DIGE gels of the hippocampi from wild type and $APP_{E693\Delta}$-transgenic mice pools were shown as Fig. 1. Two replicates of each pooled sample were run, labeling one replicate with

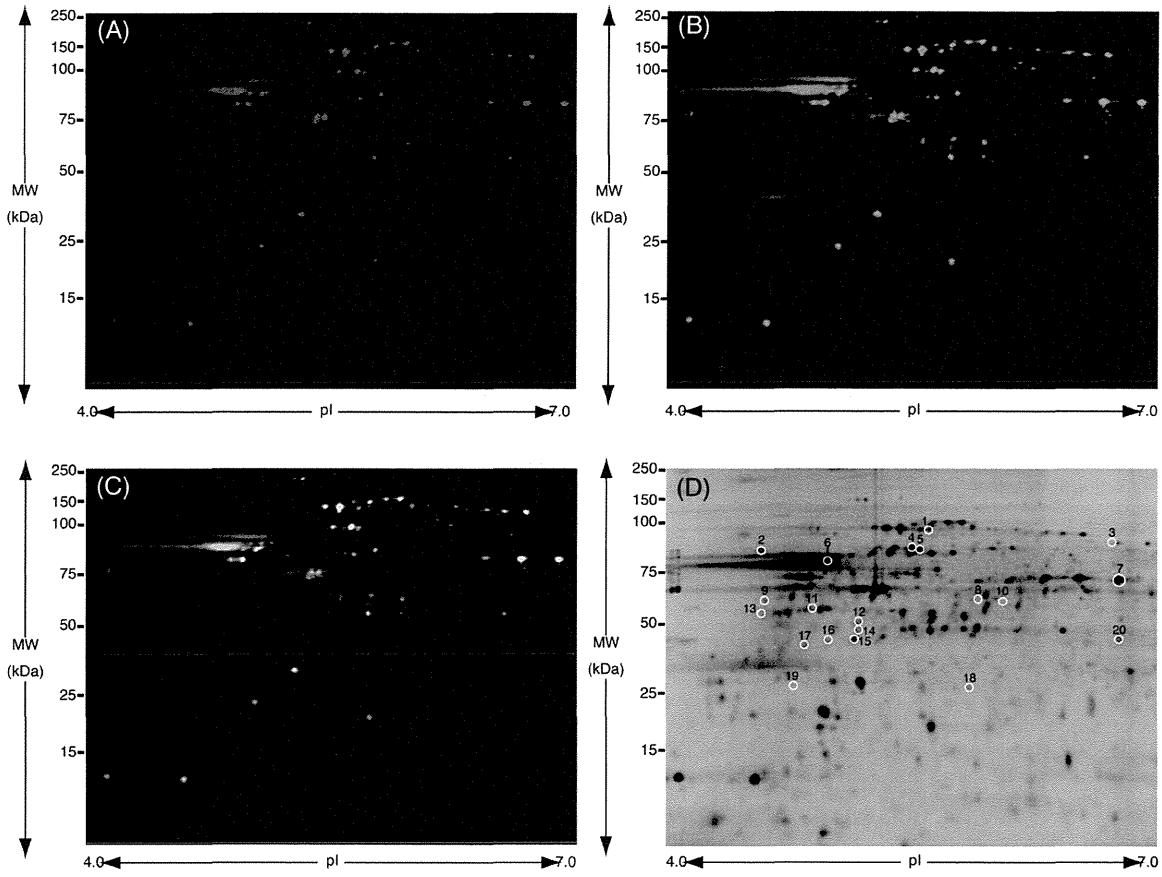

Fig. 1. 2D-DIGE gel image of fluorescence-labeled hippocampal proteins of non-transgenic and $APP_{E693\Delta}$-transgenic mice. (A) Analysis of the proteome of non-transgenic mice hippocampi with Cy3 Dye. (B) $APP_{E693\Delta}$-transgenic mice hippocampi with Cy5 Dye. (C) Merged. (D) Fourteen protein spots identified from non-transgenic and $APP_{E693\Delta}$-transgenic mice hippocampi by LC/MS/MS. Black numbers with white circles indicate proteins that are listed in Table 1.

Cy3 (Fig. 1A) and one replicate with Cy5 (Fig. 1B), resulting in three analytical gels. The 2D-DIGE comparative analysis of the wild type and $APP_{E693\Delta}$-transgenic mice revealed significant 74 spots (Fig. 1C). These spots were investigated by LC–MS/MS (Fig. 1D). Finally, fourteen proteins were identified as shown in Table 1. These proteins are classified into several groups that are involved in cytoskeletal, chaperone, energy metabolic, vesicle transport and signaling proteins (Table 2).

Spot nos. 1, 3 and 4 were identified as heat shock-related 70 kDa protein 2, stress-induced-phosphoprotein 1 and HSP60, respectively. The stress-induced-phosphoprotein 1 is the co-chaperone and thought of the function in regulation of interaction with Hsp70 and Hsp90 [10]. HSP60 is the chaperonin which is implicated in mitochondrial protein import and macromolecular assembly and may facilitate the correct folding of imported proteins [9]. The amounts of heat shock-related 70 kDa protein 2, stress-induced-phosphoprotein 1, and HSP60 were significantly decreased. On the contrary, spot no. 9 which was identified as heat shock cognate 71 kDa protein was significantly increased. This protein is also the chaperone and acts as a repressor of transcriptional activation [8]. Thus, Aβ oligomers might contribute to changing the expression of the chaperons.

Spot nos. 8, 10–12 and 16 were identified as actin, and spot nos. 15 and 17 were identified as tubulin β-2A chain. Actin is one of the major cytoskeletal proteins in neurons, and the dynamics of its assembly are involved in many aspects of cell motility, vesicle transport, and membrane turnover [14]. Actin itself is known to link with Aβ, which enhances the neurotoxicity induced by tau-mediated actin filament formation [4]. The four spots of actin but not no. 12 and those of tubulin were significantly increased. Thus, Aβ oligomers might lead to increasing the amounts of actin and tubulin.

Spot nos. 5 and 2 were identified as α-internexin and NFL, respectively, which are known as neuronal intermediate proteins [2,18]. The amounts of α-internexin and NFL were significantly decreased. Thus, the decreased amounts of NFL and internexin might raise neural dysfunction in the hippocampus of AD.

Spot nos. 7 and 13 were identified as α-enolase. Spot nos. 14 and 19 were identified as γ-enolase and ATP synthase subunit β, respectively. Enolase is a multifunctional protein as glycolytic enzyme, belonging to a novel class of surface proteins [11]. ATP synthase is a key role enzyme that provides energy for the cell to use through the synthesis of ATP [1]. The amount of α-enolase was significantly decreased, but the amounts of γ-enolase and ATP synthase subunit β were significantly increased. Interestingly, the levels of α-enolase and ATP synthase subunit α mitochondrial proteins significantly increased in the hippocampus of J20 Tg mice with amyloid deposition [19]. The amyloid deposit enhanced the expression of energy metabolic proteins [22]. Combined with our findings, both Aβ oligomers and amyloid deposition might play an important role in the change of energy metabolic proteins as α-enolase, γ-enolase and ATP synthase subunit β.

Spot no. 20 was identified as dynamin. Dynamin, a well studied neuron-specific mechanochemical GTPase, pinches off synaptic vesicles, freeing them from the membrane and allowing them to re-enter the synaptic vesicle pool to be refilled for future release

Table 1
Identified proteins from differentially expressed in the hippocampus of$APP_{E693\Delta}$-transgenic mice when compared to non-transgenic littermates.

Spot no.	Protein ID	Fold (APP/WT)	*t*-Test	Accession	Coverage	#Peptides	Predicted MW (kDa)	Calc. pI	Score
1	Heat shock-related 70 kDa protein 2	−1.32	0.040	P14659	26.22	23	69.6	5.67	625.70
2	Neurofilament light polypeptide	−1.48	0.002	P08551	39.96	43	61.5	4.64	1004.84
3	Stress-induced-phosphoprotein 1	−1.44	0.002	Q60864	16.21	9	62.5	6.80	157.49
4	60 kDa heat shock protein	−1.36	0.013	P63038	52.71	71	60.9	6.18	1916.39
5	Alpha-internexin	−1.34	0.023	P46660	42.66	39	55.7	5.27	1119.47
6	Protein kinase C and cascin kinase substrate in neurons protein 1	−1.48	0.023	Q61644	28.34	15	50.5	5.24	356.92
7	Alpha-enolase	−1.32	0.000	P17182	34.33	24	47.1	6.80	474.21
8	Actin, cytoplasmic 1	1.51	0.003	P60709	25.87	14	41.7	5.48	231.79
9	Heat shock cognate 71 kDa protein	1.35	0.015	P63017	12.54	16	70.8	5.52	319.85
10	Actin, cytoplasmic	1.34	0.004	P60709	24.27	13	41.7	5.48	279.37
11	Actin, cytoplasmic 1	1.38	0.022	P60709	15.47	7	41.7	5.48	243.14
12	Actin, cytoplasmic 1	−1.56	0.013	P60709	22.67	12	41.7	5.48	131.57
13	Gamma-enolase	1.33	0.005	P17183	20.05	13	47.3	5.11	237.25
14	ATP synthase subunit beta	1.40	0.047	P56480	23.60	18	56.3	5.34	356.19
15	Tubulin beta-2A chain	1.31	0.021	Q13885	14.83	13	49.9	4.89	313.07
16	Actin, cytoplasmic 1	1.47	0.002	P60709	6.93	3	41.7	5.48	97.01
17	Tubulin beta-2S chain	1.44	0.009	Q13885	11.46	5	49.9	4.89	118.50
18	Clathrin light chain B	1.68	0.005	P09497	8.30	3	25.2	4.64	95.06
19	ATP synthase subunit beta	1.46	0.013	P06576	16.64	16	56.5	5.40	283.06
20	Dynamin-1	1.40	0.006	Q05193	9.61	13	97.3	7.17	242.16

Mass spectrometry protein identification of 2D-DIGE spots of interest and statistical analysis using *t*-test between wild type mice and $APP_{E693\Delta}$-transgenic mice gels ($P < 0.05$). The proteins of mouse hippocampus were separated by 2DE and identified by LC MS/MS, following in-gel digestion with trypsin. The spots representing identified proteins are indicated in Fig. 1D and are designated with their ID accession numbers of Swiss Prot database. Score relates to the probability assignment. Score and sequence coverage were calculated by MASCOT search engine (http://www.matrixscience.com).

Table 2
Functions regulated by proteins that showed an altered expression in $APPE_{693\Delta}$-transgenic mouse hippocampus.

Function	Identified protein	Up/down
Cytoskeletal and their interacting proteins	Neurofilament light polypeptide	Down
	Alpha-internexin	Down
	Actin, cytoplasmic 1	Up/down
	Tubulin β-2A Chain	Up
Chaperone and their interacting proteins	Stress-induced-phosphoprotein 1	Down
	60 kDa heat shock protein	Down
	Heat shock cognate 71 kDa protein	Down
Energy metabolic proteins	Alpha-enolase	Down
	Gamma-enolase	Up
	ATP synthase subunit beta	Up
Vesicle transport and recycling	Dynamin-1	Up
	Clathrin light chain B	Up
Signaling proteins	Protein kinase C and casein kinase substrate in neurons protein 1	Down

The analysis of proteins function was done by using MOTIF (http://www.genome.jp/tools/motif/).

[12]. The amount of dynamin was significantly increased. Our findings in $APP_{E693\Delta}$-transgenic mice without plaque deposition are consistent with previous findings that protein levels of dynamin were increased in Tg2576 mice with plaque deposition [21], suggesting that the release of neurotransmitter is affected by dynamin increased irrespective of AD stage. Also, spot no. 6 was identified as Pacsin 1. The Pacsin 1 is colocalized, oligomerized and bound with dynamin, and both proteins participate in synaptic vesicle endocytosis [17]. The amount of Pacsin 1 was significantly increased. Taken together, Pacsin 1 and dynamin enhanced by Aβ oligomers

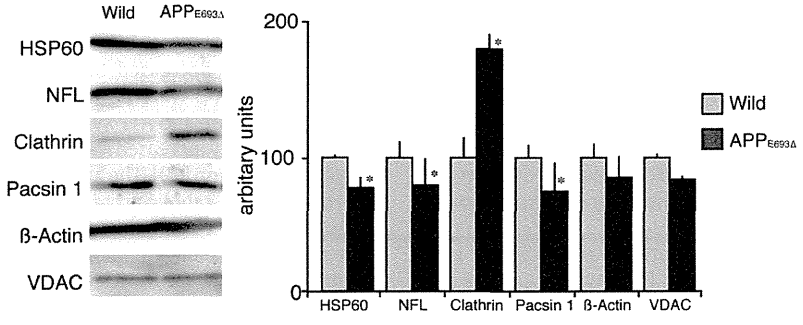

Fig. 2. Differentially expressed proteins validated by Western blotting for the hippocampus of non-transgenic and $APP_{E693\Delta}$-transgenic mice. (A) The levels of HSP60, NFL, clathrin, Pacsin 1, β-actin and VDAC in individual samples of each group were detected. (B) Graphical representation of the semi quantitative analysis (mean ± SEM of O.D. of bands). Data are presented as mean ± SEM ($n = 4$) *t*-test; $^*P < 0.05$ vs. $APP_{E693\Delta}$-transgenic mice.

might change the function of synaptic vesicle in the hippocampus of AD.

Spot no. 18 was identified as clathrin, which is known as the major protein of the polyhedral coat of coated pits and vesicles [7]. The amount of spot no. 18 was significantly decreased. APP was associated clusters of clathrin-coated vesicles and endosomes [3]. Thus, Aβ oligomers might inhibit the vesicle formation by clathrin.

In addition, we performed a validation experiment for HSP60, NFL, clathrin, Pacsin 1 and β-actin as the altered proteins, and VDAC as the unchanged protein (as control) [23]. The increased levels of clathrin, the decreased levels of HSP60, NFL, and Pacsin 1 and the unchanged level of β-actin and VDAC in $APP_{E693\Delta}$-transgenic mice hippocampus were validated by Western blotting (Fig. 2).

In summary, we identified the altered levels of 14 proteins in $APP_{E693\Delta}$-transgenic mice hippocampus using 2D-DIGE and LC–MS/MS approach. This approach elucidated the pathological effects of Aβ oligomers on hippocampus. Our findings might provide a clue for investigation of the hippocampus of AD early stage.

Acknowledgements

This work was supported by grants from Kobe Gakuin University for Collaborative Research C and the Smoking Research Foundation. The authors thank Dr. Tadanori Mayumi for his encouragement during the early days of the study.

References

[1] U. Andersson, H. Antonicka, J. Houstek, B. Cannon, A novel principle for conferring selectivity to poly(A)-binding proteins: interdependence of two ATP synthase beta-subunit mRNA-binding proteins, Biochemical Journal 346 (Pt 1) (2000) 33–39.
[2] C.L. Chien, R.K. Liem, Characterization of the mouse gene encoding the neuronal intermediate filament protein alpha-internexin, Gene 149 (1994) 289–292.
[3] A. Ferreira, A. Caceres, K.S. Kosik, Intraneuronal compartments of the amyloid precursor protein, Journal of Neuroscience 13 (1993) 3112–3123.
[4] T.A. Fulga, I. Elson-Schwab, V. Khurana, M.L. Steinhilb, T.L. Spires, B.T. Hyman, M.B. Feany, Abnormal bundling and accumulation of F-actin mediates tau-induced neuronal degeneration in vivo, Nature Cell Biology 9 (2007) 139–148.
[5] A. Gorg, C. Obermaier, G. Boguth, A. Harder, B. Scheibe, R. Wildgruber, W. Weiss, The current state of two-dimensional electrophoresis with immobilized pH gradients, Electrophoresis 21 (2000) 1037–1053.
[6] J. Hardy, D.J. Selkoe, The amyloid hypothesis of Alzheimer's disease: progress and problems on the road to therapeutics, Science 297 (2002) 353–356.
[7] J. Hirst, M.S. Robinson, Clathrin and adaptors, Biochimica et Biophysica Acta 1404 (1998) 173–193.
[8] C.R. Hunt, A.J. Parsian, P.C. Goswami, C.A. Kozak, Characterization and expression of the mouse Hsc70 gene, Biochimica et Biophysica Acta 1444 (1999) 315–325.
[9] S. Ikawa, R.A. Weinberg, An interaction between p21ras and heat shock protein hsp60, a chaperonin, Proceedings of the National Academy of Sciences 89 (1992) 2012–2016.
[10] J.L. Johnson, A. Halas, G. Flom, Nucleotide-dependent interaction of Saccharomyces cerevisiae Hsp90 with the cochaperone proteins Sti1, Cpr6, and Sba1, Molecular and Cellular Biology 27 (2007) 768–776.
[11] M. Kaghad, X. Dumont, P. Chalon, J.M. Lelias, N. Lamande, M. Lucas, M. Lazar, D. Caput, Nucleotide sequences of cDNAs alpha and gamma enolase mRNAs from mouse brain, Nucleic Acids Research 18 (1990) 3638.
[12] B.L. Kelly, R. Vassar, A. Ferreira, Beta-amyloid-induced dynamin 1 depletion in hippocampal neurons. A potential mechanism for early cognitive decline in Alzheimer disease, Journal of Biological Chemistry 280 (2005) 31746–31753.
[13] W.L. Klein, G.A. Krafft, C.E. Finch, Targeting small Abeta oligomers: the solution to an Alzheimer's disease conundrum? Trends in Neurosciences 24 (2001) 219–224.
[14] T.B. Kuhn, P.J. Meberg, M.D. Brown, B.W. Bernstein, L.S. Minamide, J.R. Jensen, K. Okada, E.A. Soda, J.R. Bamburg, Regulating actin dynamics in neuronal growth cones by ADF/cofilin and rho family GTPases, Journal of Neurobiology 44 (2000) 126–144.
[15] V.M. Lee, M. Goedert, J.Q. Trojanowski, Neurodegenerative tauopathies, Annual Review of Neuroscience 24 (2001) 1121–1159.
[16] S. Li, S. Hong, N.E. Shepardson, D.M. Walsh, G.M. Shankar, D. Selkoe, Soluble oligomers of amyloid Beta protein facilitate hippocampal long-term depression by disrupting neuronal glutamate uptake, Neuron 62 (2009) 788–801.
[17] J. Modregger, B. Ritter, B. Witter, M. Paulsson, M. Plomann, All three PACSIN isoforms bind to endocytic proteins and inhibit endocytosis, Journal of Cell Science 113 (Pt 24) (2000) 4511–4521.
[18] R.A. Nixon, R.K. Sihag, Neurofilament phosphorylation: a new look at regulation and function, Trends in Neurosciences 14 (1991) 501–506.
[19] R.A. Robinson, M.B. Lange, R. Sultana, V. Galvan, J. Fombonne, O. Gorostiza, J. Zhang, G. Warrier, J. Cai, W.M. Pierce, D.E. Bredesen, D.A. Butterfield, Differential expression and redox proteomics analyses of an Alzheimer disease transgenic mouse model: effects of the amyloid-beta peptide of amyloid precursor protein, Neuroscience 177 (2011) 207–222.
[20] D.J. Selkoe, Alzheimer's disease is a synaptic failure, Science 298 (2002) 789–791.
[21] S.J. Shin, S.E. Lee, J.H. Boo, M. Kim, Y.D. Yoon, S.I. Kim, I. Mook-Jung, Profiling proteins related to amyloid deposited brain of Tg2576 mice, Proteomics 4 (2004) 3359–3368.
[22] R. Sultana, D. Boyd-Kimball, J. Cai, W.M. Pierce, J.B. Klein, M. Merchant, D.A. Butterfield, Proteomics analysis of the Alzheimer's disease hippocampal proteome, Journal of Alzheimer's Disease 11 (2007) 153–164.
[23] M. Takano, K. Maekura, M. Otani, K. Sano, T. Nakamura-Hirota, S. Tokuyama, K.S. Min, T. Tomiyama, H. Mori, S. Matsuyama, Proteomic analysis of the brain tissues from a transgenic mouse model of amyloid beta oligomers, Neurochemistry International 61 (2012) 347–355.
[24] M. Takano, M. Otani, A. Sakai, K. Kadoyama, S. Matsuyama, A. Matsumoto, M. Takenokuchi, M. Sumida, T. Taniguchi, Use of a phosphosensor dye in proteomic analysis of human mutant tau transgenic mice, Neuroreport 20 (2009) 1648–1653.
[25] T. Tomiyama, S. Matsuyama, H. Iso, T. Umeda, H. Takuma, K. Ohnishi, K. Ishibashi, R. Teraoka, N. Sakama, T. Yamashita, K. Nishitsuji, K. Ito, H. Shimada, M.P. Lambert, W.L. Klein, H. Mori, A mouse model of amyloid beta oligomers: their contribution to synaptic alteration, abnormal tau phosphorylation, glial activation, and neuronal loss in vivo, Journal of Neuroscience 30 (2010) 4845–4856.

Laboratory of Biopharmaceutical Research[1], National Institute of Biomedical Innovation; Laboratory of Toxicology and Safety Science[2], Graduate School of Pharmaceutical Sciences, Osaka University; The Center for Advanced Medical Engineering and Informatics[3], Osaka University; Department of Biochemistry[4], Osaka Medical Center for Cancer and Cardiovascular Diseases; Section of Laboratory Equipment[5], National Institute of Biomedical Innovation; Laboratory of Biomedical Innovation[6], Graduate School of Pharmaceutical Sciences, Osaka University, Osaka, Japan

Epidermal growth factor receptor localized to exosome membranes as a possible biomarker for lung cancer diagnosis

T. YAMASHITA[1,2,*], H. KAMADA[1,3,*], S. KANASAKI[1,2], Y. MAEDA[1,2], K. NAGANO[1], Y. ABE[1], M. INOUE[1], Y. YOSHIOKA[1,2,3], Y. TSUTSUMI[1,2,3], S. KATAYAMA[1,5], M. INOUE[4], S. TSUNODA[1,3,5,6]

Received March 11, 2013, accepted April 26, 2013

Shin-ichi Tsunoda, Ph.D, Laboratory of Biopharmaceutical Research, National Institute of Biomedical Innovation, 7-6-8 Saito-Asagi, Ibaraki, Osaka 567-0085, Japan.
tsunoda@nibio.go.jp
[*] *These authors contributed equally to the work.*

Pharmazie 68: 969–973 (2013) *doi: 10.1691/ph.2013.3599*

Detection of drug-target proteins and biomarkers that are expressed in cancer tissue has significant potential for both diagnosis and treatment of cancer. However, current immuno-histochemical and cytogenetic analyses of biopsy specimens for pre-operational diagnosis are highly invasive and often difficult to apply to lung cancer patients. The purpose of this study was to evaluate the possible utility of determining epidermal growth factor receptor (EGFR) expression on exosomal membranes using a targeted ELISA with an anti-CD81 antibody as a capture antibody for lung cancer diagnosis. While soluble EGFR (sEGFR) levels in plasma were not remarkably different between lung cancer patients and normal controls, significantly higher exosomal EGFR expression levels were observed in 5/9 cancer cases compared to normal controls. These results suggest that measurement of exosomal protein levels could be useful for *in vitro* diagnosis, and that exosomal EGFR is a possible biomarker for characterization of lung cancer.

1. Introduction

Lung cancer has been recognized as a heterogeneous disease, since its development is unique in terms of clinical characterizations, prognosis, response and tolerance to treatment for every patient. Epidermal growth factor receptor (EGFR) expression is significantly elevated in some of the tumors and has been associated with tumor growth, invasion, and metastasis in non-small cell lung cancer. The function of EGFR is up-regulated in lung cancers and thus its blockade by EGFR tyrosine kinase inhibitors (TKI) improves outcomes for lung cancer patients. Therefore expression of EGFR could possibly serve as a marker to predict which lung cancer patients would be most likely benefit from such a treatment (Philip et al. 2011; Gusterson et al. 1984; Modjtahedi et al. 1993). Although tumor biopsy is currently recommended as the standard method to detect EGFR expression in patients, it has several disadvantages such as its high invasiveness, potential sampling error and risk of trauma. Considering these limitations, there is a need to develop novel and less invasive methods to detect lung cancer.

Exosomes are endogenous nano-vesicles (40–100 nm in diameter) secreted by various cells (Deng et al. 2012; Simons and Raposo 2009; Théry et al. 2009) and they are known to contain many kinds of RNAs and proteins derived from their parent cells. Micro RNAs (miRNAs) included in blood exosomes could potentially be used for cancer diagnosis (Kosaka et al. 2010). The membranes of exosomes secreted from cancer cells contain proteins related to characteristics of specific cancers such as melanoma and colon cancer (Mathivanan et al. 2010; Simpson et al. 2008). These observations support the idea that detection of exosomal EGFR as a blood biomarker could prove useful for cancer diagnosis and characterization. In this study, we established a simple ELISA method to detect and quantify exosomal EGFR. We also examined the possibility of utilizing exosomal EGFR as a blood biomarker for lung cancer diagnosis. Our demonstration of exosomal EGFR in the plasma from a lung cancer patient provides a rationale for further studies to investigate the utility of exosomal EGFR as an easily measurable biomarker for lung cancer diagnosis.

2. Investigations and results

2.1. Characteristics of exosomes derived from HPAEpiC and HARA-B cell lines

Exosomes derived from HPAEpiC and HARA-B cells were compared using transmission electron microscopy (TEM) and dynamic light scattering. Electron microscopy analysis revealed that the exosomes collected from the culture medium of various cancer cell lines consisted primarily of small membrane vesicles having an average diameter of 90–120 nm (Fig. 1A, 1B), similar to previously described exosome preparations (Valadi et al. 2007).

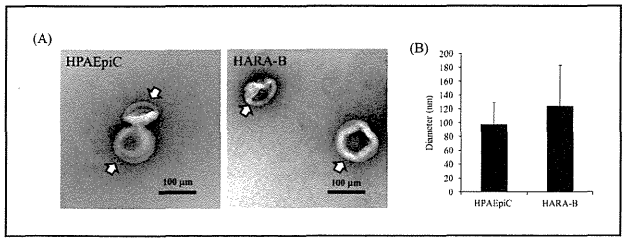

Fig. 1: Characteristics of purified exosomes. A) TEM images of exosomes derived from HPAEpiC and HARA-B cells negatively stained with uranyl acetate. B) The average diameters of exosomes. The average particle diameters obtained by dynamic light scattering. Data are shown as means and standard deviations of 6 measurements.

2.2. Comparison of EGFR expression between cancer cell lines

In order to select lung cancer cells that expressed EGFR at high levels, western blots were performed for cancer cell lines and HPAEpiC cells (Fig. 2A). Quantitative analysis revealed that lung cancer cell lines expressed EGFR while EGFR was seldom detected on HPAEpiC cells. EGFR expression was particularly high on HARA-B cells (Fig. 2B). Furthermore, EGFR expression levels were parallel on exosomes and the cells from which they were derived (Fig. 2B and 2C).

2.3. Expression analysis of exosomal EGFR derived from conditioned media and plasma of tumor-bearing mice

Detection, quantification and characterization of target molecules by a blood test is ideal for performing a cancer diagnosis. To determine whether EGFR was expressed on the exosomes derived from cancer cells and whether this could be a useful biomarker indicating the presence or the expression level of the cancer-related molecules of cancer, exosomal EGFR levels in conditioned media and plasma from tumor-bearing mice were measured by an ELISA assay. At first, purified exosomes derived from cell culture supernatants were captured using an anti-human CD81 antibody. Furthermore, Figs. 3A and 3B show that EGFR in cell supernatants and purified exosomes derived from HARA-B cells, which showed the highest levels of EGFR among the examined cell lines (Fig. 2C), were detected in a dose-dependent manner. In contrast, EGFR expression on exosomes derived from HPAEpiC cells was almost undetectable. Thus, exosomal EGFR expression in cell supernatants could be assessed by this ELISA system. Next, the exosomal EGFR levels in plasma of HARA-B tumor-bearing mice were investigated. Expression of EGFR in HARA-B tumor tissue was confirmed by immunostaining using an anti-human EGFR antibody (Fig. 3C). The plasma samples of the tumor-bearing mice were measured using an established ELISA, and then exosomal EGFR levels were found to increase in parallel with the tumor size (Fig. 3D). These results indicate that detection of exosomal EGFR levels in plasma could be used to estimate the sizes of tumors.

2.4. Comparison of soluble and exosomal EGFR levels in human plasma

A previous study has indicated that sEGFR is not a useful blood biomarker for lung cancer diagnosis because it is detected in blood from both healthy individuals and cancer patients (Jacot et al. 2004). Therefore, in order to evaluate the possible utility of exosomal EGFR as a lung cancer biomarker, we compared the expression levels of soluble and exosomal EGFR in plasma from nine lung cancer patients and from normal controls. The sEGFR levels did not differ remarkably between normal and lung cancer

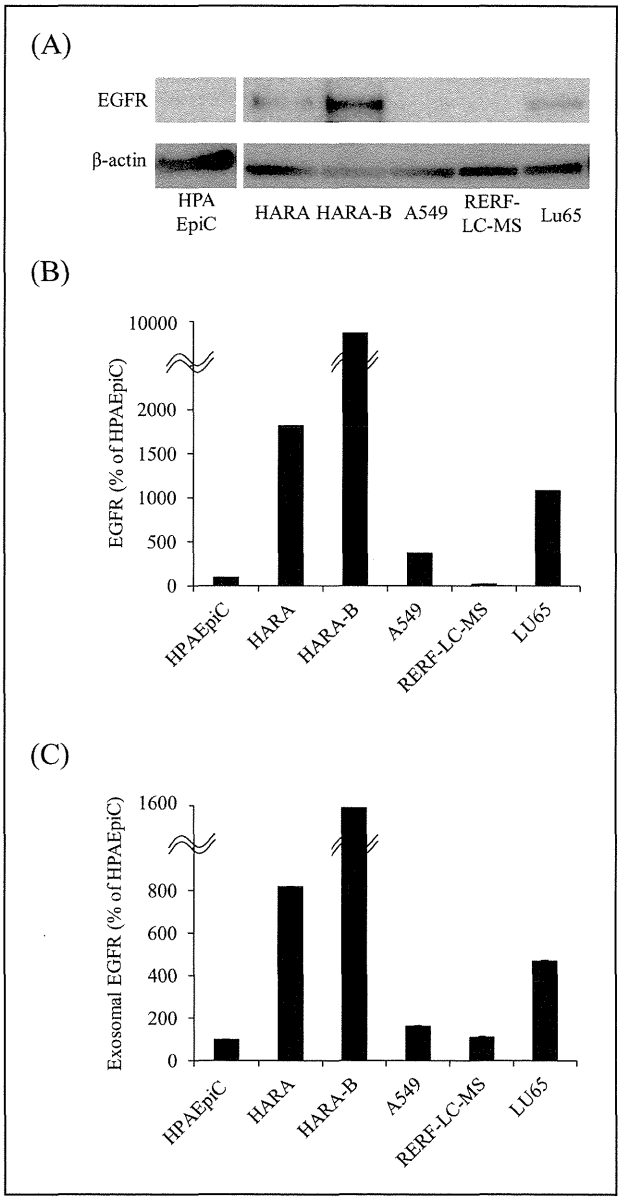

Fig. 2: Expression of EGFR on cancer cell-derived exosomes. A) Western blotting analysis of EGFR expression in lysates from lung cancer cell lines. B) Quantitative analysis of the Western blotting results of A. Signal quantification was performed by densitometry with normalization by b-actin. C) Expression of EGFR on exosomes in conditioned media. Ultracentrifuge-purified exosomes derived from the indicated cells were captured by anti-CD81 and detected by anti-EGFR. Data are shown as means and standard deviations (n = 3).

patient plasma. On the other hand, exosomal EGFR was significantly higher in five lung cancer patients plasma compared to healthy controls.

3. Discussion

Several blood biomarkers are commonly used for clinical cancer detection, e.g., carcinoembryonic antigen (CEA) and cytokeratin 19 fragment (CYFRA 21–1) for lung cancer (MacSween et al. 1972; Pujol et al. 1993). However, these biomarkers show low specificity and poor capability to detect tumors, although they continue to be used for cancer diagnosis. There is a clear need for improved biomarkers with higher specificity for cancer diagnosis and therapy. EGFR is known to be a good biomarker for lung cancer because it is highly expressed in tumor tissue

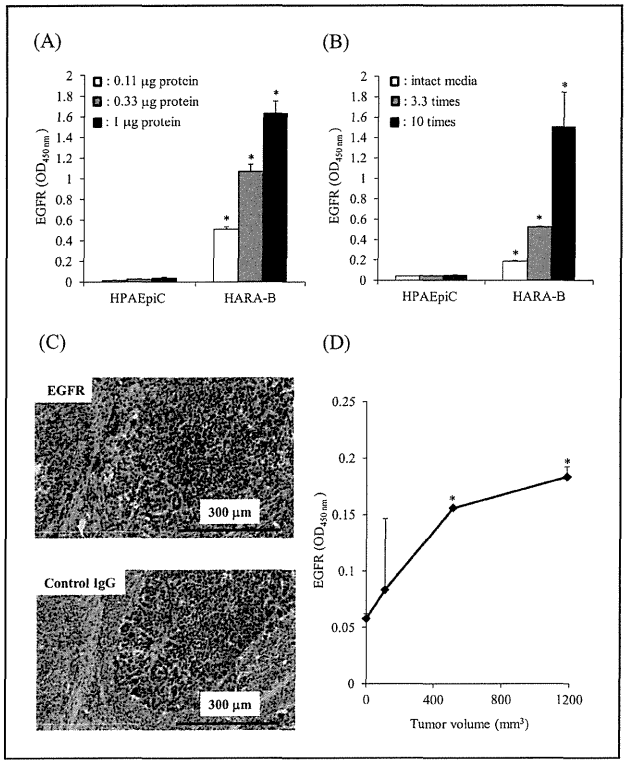

Fig. 3: Exosomal EGFR derived from conditioned medium and plasma from tumor-bearing mice. A) Concentration dependence analysis of EGFR expression on ultracentrifuge-purified exosomes (0.11, 0.33 and 1.0 μg exosomal protein) derived from HARA-B cells. Exosomes were captured and detected using an anti-CD81 antibody B) EGFR expression in exosomes derived from conditioned media of HARA-B cells (intact and concentrated 3 and 10 times by ultrafiltration). Exosomes were captured by an anti-CD81 antibody and then detected using an anti-EGFR antibody. C) Expression of EGFR on HARA-B xenograft tumors. The HARA-B tumor sections were stained using an anti-EGFR antibody. Isotype control staining was also performed. Representative 200x photomicrographs are shown. D) Relationship between plasma levels of CD81 + /EGFR + exosomes and tumor volume. Plasma samples were collected from mice sacrificed 10, 17 and 21 days after inoculation with HARA-B cells. Data are shown as means and standard deviations (n = 3).

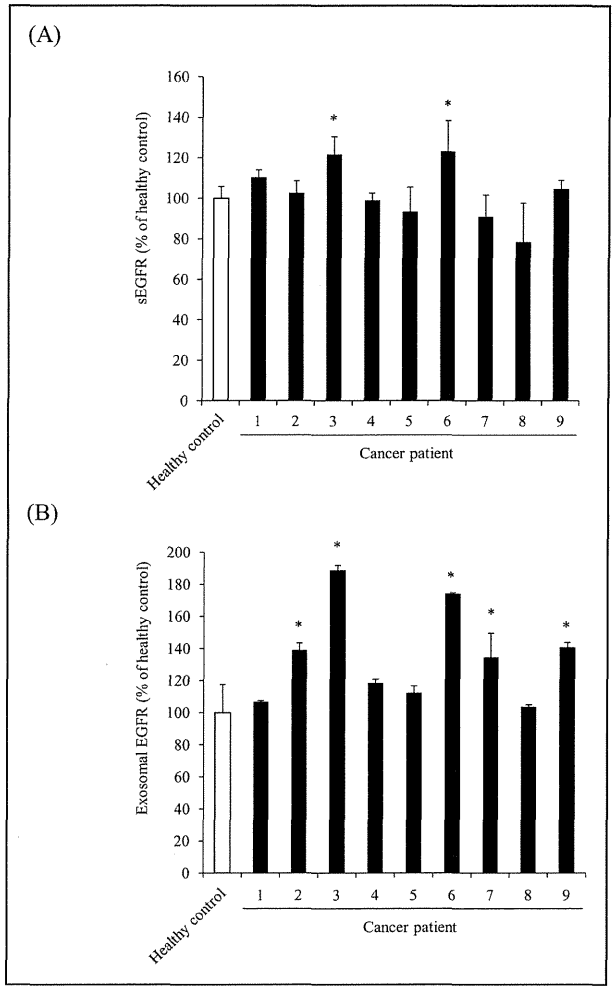

Fig. 4: Expression of sEGFR and exosomal EGFR in human plasma from lung cancer patients. A) Expression analysis of sEGFR using an ELISA, which consisted of two different antibodies recognizing other epitopes of EGFR. B) Expression analysis of exosomal EGFR using an ELISA, which utilized anti-EGFR and anti-CD81 antibodies. Exosomes were captured by an anti-CD81 antibody and then detected using an anti-EGFR antibody. Data are shown as means and standard deviations (n = 3). *$P < 0.05$ (vs. normal).

and also is a target molecule of EGFR TKIs, which are used to treat lung cancer patients. However, EGFR expression is evaluated by performing a biopsy that is highly invasive, and it would be quite desirable to develop a less invasive method to quantify it. The present study demonstrates that exosomal EGFR is a possible biomarker for lung cancer detection and characterization, and its expression may be evaluated by an EGFR-targeted ELISA using an anti-CD81 antibody as a capture antibody. This ELISA system should be capable of detecting EGFR on membranes of exosomes. This diagnostic method could be applied to lung cancer detection and pharmacometrics analysis, etc.

A previous report showed that the levels of exosomes in blood derived from cancer patients are higher than in healthy persons (Taylor and Gercel-Taylor 2008). Therefore, an ELISA system could be used for lung cancer diagnostics if EGFR was expressed at higher levels on exosomes from lung cancer patients. However, it has been reported that sEGFR levels are similar in blood from lung cancer patients and normal controls. Furthermore, exosomes are detected in plasma from healthy individuals as well as from cancer patients because they are secreted from various cells in normal and disease situations (Fevrier et al. 2004; Witek et al. 2009). Therefore, the tumor-derived exosomes must be distinguished from other exosomes for diagnostic purposes. The results of our animal study indicate that exosomes in plasma that express high levels of EGFR are clearly derived from tumor tissue, because this mouse model was inoculated with a human lung cancer cell line and the ELISA system can only detect human CD81 and human EGFR. Furthermore, our results indicate that exosomal EGFR detection could potentially be used in blood tests to diagnose lung cancer because the exosomal EGFR level was higher in lung cancer patients than in normal individuals (Fig. 4).

It is thought that secretion of exosomal EGFR derived from tumor tissue is increased in lung cancer patients. However, the present study did not reveal any relationship between EGFR expression levels in exosomes *versus* tumor tissues. Further studies are necessary to investigate the relationships among size, stage, EGFR expression of tumor tissues and plasma exosomal EGFR levels. Future large-scale validation studies are also anticipated. Tetraspanins such as CD9, CD63 and CD81 are a family of small proteins expressed on membranes. They are highly enriched in late endosomes, lysosomes, and multi-vesicular bodies, where they associate to form complexes (Andre et al. 2002; Abache et al. 2007; Pols and Klumperman 2009). Secretion of exosomes from dendritic cells of CD9 knockout mice was found to be reduced (Chairoungdua et al. 2010), suggesting that tetraspanins are essential molecules for generation of exosomes. Another study utilized an anti-CD63 antibody and caveolin-1 antibodies to detect endosomes in plasma from melanoma

patients (Logozzi et al. 2009). CD63-positive exosomes were found to be highly expressed in *in vitro* culture supernatants and were also detected in plasma from melanoma patients. In contrast, we carried out a proteomics study to determine what kinds of tetraspanins were expressed on exosomes derived from lung cancer cell lines. The results indicated that exosomal CD63 was seldom detected in some lung cancer cells but CD81 was widely expressed (in the lines HARA, HARA-B, A549, and LU65). Chiba et al. also reported that CD81 was widely expressed on exosomes derived from colon cancer cell lines (HCT-15, SW480, and WiDr), as indicated by western blotting experiments (Chiba et al. 2012). Furthermore, it was reported that CD81 promotes cell proliferation by ERK/MAP Kinase activation and tyrosine phosphorylation in hepatocellular carcinoma cells (Carloni et al. 2004). Thus, CD81 may be useful as an appropriate marker for exosomes derived from cancer cells.

This study demonstrates for the first time that exosomal EGFR may be detected and quantified using CD81 and EGFR targeted ELISA assays. The alteration of plasma EGFR concentration in cancer patients could be detected by a targeted ELISA capturing exosomes because soluble EGFR is usually observed in the healthy state. Although this ELISA system could be useful for cancer detection, optimization of this method (e.g. exploitation of radio-isotopes or fluorescence, affinity maturation of antibodies, etc.) will be needed to estimate EGFR expression levels in cancer tissues.

It has been reported that tumor-specific gene mutations of EGFR could be detected by reverse transcription-PCR analysis in serum vesicles from glioblastoma patients (Skog et al. 2008). The exosomes include not only tumor derived membrane or cytosolic proteins but also mRNA expressed in tumor cells. In the future, exosome analysis, which allows simultaneous measurement of EGFR gene mutations and EGFR protein expression, will likely provide more valuable information for diagnosis and to inform therapeutic decisions for cancer patients, compared to previous methods.

4. Experimental

4.1. Cell lines

HARA, HARA-B, A549, RERF-LC-MS and LU65 cells were purchased from the JCRB cell bank. HARA, HARA-B and LU65 cells were maintained in RPMI1640 medium containing 10% fetal calf serum (FCS). A549 and RERF-LC-MS cells were maintained in Eagle's minimal essential medium with non-essential amino acids containing 10% FCS under a 5% CO_2 atmosphere at 37 °C. Primary human pulmonary alveolar epithelial cells (HPAEpiC) were purchased from Science Cell Research Laboratory. These cells were maintained in Alveolar Epithelial Cell Medium (Science Cell Research Laboratory, California, USA) under a 5% CO_2 atmosphere at 37 °C.

4.2. Electron microscopy

Electron microscope images of exosomes were taken by floating a carbon-coated 400-mesh Formvar EM grid on top of 5 μl of freshly prepared exosomes in deionized water for 20 min. The grid was then briefly washed with deionized water and floated on a drop of 2% uranyl acetate. Samples were examined using an H-7650 Transmission Electron Microscope (Hitachi High-Technologies).

4.3. Preparation of conditioned media and exosomes

Prior to exosomes collection, confluent cells were incubated for 72 h without FCS. Exosomes were prepared from the supernatant of lung cancer cells and HPAEpiC by centrifugation. Six hundred ml volumes of supernatants containing 1 x 10^8 HPAEpiC or 6 x 10^8 lung cancer cells were centrifuged at 300 g for 5 min to eliminate cells and at 16,000 x g for 20 min, followed by filtration through a 0.22 μm filter to clear cell debris. Exosomes were precipitated by ultracentrifugation at 140,000 x g for 70 min. The pellets of exosomes were washed once in PBS and their protein contents were measured using a Micro BCA protein assay kit (Thermo Fisher Scientific). Particle sizes were measured by dynamic light scattering using a Zetasizer nano (Malvern).

4.4. Western blots

All cells were lysed in RIPA buffer (Thermo Fisher Scientific) containing Complete Protease Inhibitor Cocktail (Roche Diagnostics). Determination of protein concentrations was performed using a micro BCA protein assay kit (Thermo Fisher Scientific). Cell lysates were electrophoresed in 10% SDS-polyacrylamide gels (10 μg/ lanes) and transferred to PVDF membranes (Millipore). After blocking with 4% Block Ace (DS Pharma Biomedical) for 60 min at room temperature, the blots were reacted with anti-EGFR polyclonal antibody (clone AF231, R&D Systems) in a buffer containing 0.4% block ace, and then with an HRP conjugated anti-goat IgG secondary antibody (Jackson Immuno Research) in the same buffer and detected using the ECL-plus system (GE Healthcare). Equal amounts of protein loading were confirmed by parallel β-actin immunoblotting, and signal quantification was performed by densitometric scanning.

4.5. Detection of exosomes in plasma and conditioned media using targeted ELISA with anti CD81 and anti EGFR antibody

Ninety-six well Maxisorp plates (Nunc) were coated with 20 μg/ml mouse anti human CD81 monoclonal antibody (clone 1D6, Gene Tex) in volumes of 100 μl/well of carbonate buffer (pH 9.6) and incubated overnight at 4 °C. After incubation, 100 μl/well of 4% BLOCK ACE (DS-pharma) were added and incubated overnight at 4 °C. After 3 washes with PBS, several concentrations of purified exosomes, conditioned media and mouse or human plasma were added to a final volume of 100 μl and incubated for 60 min at 37 °C. Sample concentrations are given in the figure legends. After 3 washes with PBS, 0.8 μg/ml goat anti-human EGFR polyclonal antibody was added and incubated for 60 min at 37 °C. After 3 washes with PBS, the plates were incubated with 100 μl of HRP-conjugated anti-goat IgG antibody per well diluted 1:5,000 in 0.4% block ace for 60 min at room temperature. After the final 3 washes with PBS, the reaction was developed with tetramethyl benzidine reagents, blocked with H_2SO_4 and optical densities were recorded at 450 nm. Human plasma samples were purchased from Kohjin Bio (Saitama, Japan: healthy control) and Tissue Solutions Ltd (Glasgow, UK: lung cancer samples). Soluble EGFR (sEGFR) was detected by EGFR Human ELISA kit (R & D Systems).

4.6. Human tumor xenograft mice model

Six-week-old male BALB/c Slc-nu/nu mice (Japan SLC) were maintained at the animal care facility of National Institute of Biomedical Innovation under a regulated protocol. A suspension of HARA-B cells (1 x 10^6 cells/mouse) was inoculated s.c. into the backs of the mice. The two perpendicular diameters of the tumors were obtained using a slide caliper 10, 17 and 21 days after inoculation and then tumor volumes were calculated using the formula 0.5 x (A x B^2), where A and B are the longest and shortest dimensions of the tumor, respectively (Andre et al. 2002). Six-hundred microliters of plasma were collected from tumor-bearing mice sacrificed at 10, 17 and 21 days after inoculation.

4.7. Immunohistochemistry staining

Frozen HARA-B tumor tissues in 5 μm thick sections were fixed in 4% paraformaldehyde for 15 min at 4 °C. Heat-induced epitope retrieval was performed in the Target Retrieval Solution pH 9 (Dako) according to the manufacturer's instructions. After the epitope retrieval, endogenous peroxidase was blocked with the Peroxidase Blocking Reagent (Dako). Following peroxidase blocking, the slides were incubated with 10% BSA solution for 30 min at room temperature. After BSA blocking, the slides were incubated for 60 min with goat anti human EGFR polyclonal antibody, 5 μg/ml in 3% BSA at room temperature. After 3 washes with Wash Buffer (Dako), each slide was incubated for 60 min with HRP-conjugated anti-goat IgG antibody diluted 1:1,000 in 3% BSA at room temperature. After the final 3 washes with wash buffer, the slides were stained with 3,3'-diaminobenzidine. After development, the slides were lightly counterstained with Mayer's hematoxylin. All procedures were performed using AutoStainer (Dako).

4.8. Statistical analysis

Statistical significance in ELISA signals between the control and target groups was analyzed using the one-way ANOVA followed by Tukey post-hoc test.

Acknowledgements: This study was supported in part by Grants-in-Aid for Scientific Research from the Ministry of Education, Culture, Sports, Science and Technology of Japan, and from the Japan Society for the Promotion of

Science (JSPS). This study was also supported in part by Health Labor Sciences Research Grants from the Ministry of Health, Labor and Welfare of Japan.

References

Abache T, Le Naour F, Planchon S, Harper F, Boucheix C, Rubinstein E (2007) The transferrin receptor and the tetraspanin web molecules CD9, CD81, and CD9P-1 are differentially sorted into exosomes after TPA treatment of K562 cells. J Cell Biochem 102: 650–664.

Andre F, Schartz NE, Movassagh M, Flament C, Pautier P, Morice P, Pomel C, Lhomme C, Escudier B, Le Chevalier T, Tursz T, Amigorena S, Raposo G, Angevin E, Zitvogel L (2002) Malignant effusions and immunogenic tumour-derived exosomes. Lancet 360: 295–305.

Carloni V, Mazzocca A, Ravichandran KS (2004) Tetraspanin CD81 is linked to ERK/MAPKinase signaling by Shc in liver tumor cells. Oncogene 23: 1566–1574.

Chairoungdua A, Smith DL, Pochard P, Hull M, Caplan MJ (2010) Exosome release of beta-catenin: a novel mechanism that antagonizes Wnt signaling. J Cell Biol 190: 1079–1091.

Chiba M, Kimura M, Asari S (2012) exosomes secreted from human colorectal cancer cell lines contain mRNAs, microRNAs and natural antisense RNAs, that can transfer into the human hepatoma HepG2 and lung cancer A549 cell lines. Oncol Rep 28: 1551–1558.

Deng Z, Cheng Z, Xiang X, Yan J, Zhuang X, Liu C, Jiang H, Ju S, Zhang L, Grizzle W, Mobley J, Roman J, Miller D, Zhang HG (2012) Tumor cell cross talk with tumor-associated leukocytes leads to induction of tumor exosomal fibronectin and promotes tumor progression. Am J Pathol 180: 390–398.

Fevrier B, Vilette D, Archer F, Loew D, Faigle W, Vidal M, Laude H, Raposo G (2004) Cells release prions in association with exosomes. Proc Natl Acad Sci U S A 101: 9683–9688.

Gusterson B, Cowley G, Smith JA, Ozanne B (1984) Cellular localisation of human epidermal growth factor receptor. Cell Biol Int Rep 8: 649–658.

Jacot W, Pujol JL, Boher JM, Lamy PJ (2004) Serum EGF-receptor and HER-2 extracellular domains and prognosis of non-small-cell lung cancer. Br J Cancer 91: 430–433.

Kosaka N, Iguchi H, Yoshioka Y, Takeshita F, Matsuki Y, Ochiya T (2010) Secretory mechanisms and intercellular transfer of microRNAs in living cells. J Biol Chem 285: 17442–17452.

Logozzi M, De Milito A, Lugini L, Borghi M, Calabrò L, Spada M, Perdicchio M, Marino ML, Federici C, Iessi E, Brambilla D, Venturi G, Lozupone F, Santinami M, Huber V, Maio M, Rivoltini L, Fais S (2009) High levels of exosomes expressing CD63 and caveolin-1 in plasma of melanoma patients. PLoS One 4: e5219.

MacSween JM, Warner NL, Bankhurst AD, Mackay IR (1972) Carcinoembryonic antigen in whole serum. Br J Cancer 26: 356–360.

Mathivanan S, Lim JW, Tauro BJ, Ji H, Moritz RL, Simpson RJ (2010) Proteomics analysis of A33 immunoaffinity-purified exosomes released from the human colon tumor cell line LIM1215 reveals a tissue-specific protein signature. Mol Cell Proteomics 9: 197–208.

Modjtahedi H, Eccles SA, Box G, Styles J, Dean CJ (1993) Antitumor activity of combinations of antibodies directed against different epitopes on the extracellular domain of the human EGF receptor. Cell Biophys 22: 129–146.

Philip R, Carrington L, Chan M (2011) US FDA perspective on challenges in co-developing *in vitro* companion diagnostics and targeted cancer therapeutics. Bioanalysis 3: 383–389.

Pols MS, Klumperman (2009) Trafficking and function of the tetraspanin CD63. Exp Cell Res 315: 1584–1592.

Pujol JL, Grenier J, Daurès JP, Daver A, Pujol H, Michel FB (1993) Serum fragment of cytokeratin subunit 19 measured by CYFRA 21–1 immunoradiometric assay as a marker of lung cancer. Cancer Res 53: 61–66.

Simons M, Raposo G (2009) Exosomes–vesicular carriers for intercellular communication. Curr Opin Cell Biol 21: 575–581.

Simpson RJ, Jensen SS, Lim JW (2008) Proteomic profiling of exosomes: current perspectives. Proteomics 8: 4083–4099.

Skog J, Würdinger T, van Rijn S, Meijer DH, Gainche L, Sena-Esteves M, Curry WT Jr, Carter BS, Krichevsky AM, Breakefield XO (2008) Glioblastoma microvesicles transport RNA and proteins that promote tumour growth and provide diagnostic biomarkers. Nat Cell Biol 10: 1470–1476.

Taylos DD, Gercel-Taylos C (2008) MicroRNA signatures of tumor-derived exosomes as diagnostic biomarkers of ovarian cancer. Gynecol Oncol 110: 13–21.

Théry C, Ostrowski M, Segura E (2009) Membrane vesicles as conveyors of immune responses. Nat Rev Immunol 9: 581–593.

Valadi H, Ekström K, Bossios A, Sjöstrand M, Lee JJ, Lötvall JO (2007) Exosome-mediated transfer of mRNAs and microRNAs is a novel mechanism of genetic exchange between cells. Nat Cell Biol 9: 654–659.

Witek RP, Yang L, Liu R, Jung Y, Omenetti A, Syn WK, Choi SS, Cheong Y, Fearing CM, Agboola KM, Chen W, Diehl AM (2009) Liver cell-derived microparticles activate hedgehog signaling and alter gene expression in hepatic endothelial cells. Gastroenterology 136: 320–330 e2.

Liver-specific microRNAs as biomarkers of nanomaterial-induced liver damage